NTNU
Norwegian University of
Science and Technology

Mechanical behaviour of sacrificial sandwich panels

Olav Ingvaldsen Bengtson

Department of Structural Engineering
Faculty of Engineering Science and Technology
NTNU- Norwegian University of Science and Technology

MASTER THESIS 2016

SUBJECT AREA:	DATE:	NO. OF PAGES:
Computational Mechanics	June 2016	10 + 75 +1

TITLE:

Mechanical behaviour of sacrificial sandwich panels

BY:

Olav Ingvaldsen Bengtson

SUMMARY:
The main objective of this thesis is to conduct a numerical study of sacrificial sandwich panels with aluminium foam core. This is done in order to understand how different parameters affect the energy absorption when subjected to blast load and low-velocity impact. The sacrificial sandwich panels are made up of an aluminium foam core, and aluminium face sheets on each side. The face sheets have remained the same throughout the study, while the thickness and density of the foam core have been varied.

The Numerical models are established in LS-DYNA to replicate laboratory experiments in a drop tower and in the SIMLab ShockTube. Parametric studies were conducted to investigate the effect of varying foam core thickness and density. Laboratory experiments were conducted to validate the results of the parametric studies. The results of this validation showed that the blast loaded model replicated the correct trends, while there was larger problems with the model of the low-velocity impact.

Foam core sacrificial sandwich plates show good potential for absorbing energy from blast loads. Especially low-density foam shows potential for limiting the deformation while absorbing the energy. For low-velocity impact, further work is needed to conduct proper parametric studies, but experiments show promise of good results for low-density foam.

MASTER'S THESIS 2016

for

Olav Ingvaldsen Bengtson

Mechanical behaviour of sacrificial sandwich panels

1. INTRODUCTION

In the event of high-energy accidents and targeted attacks, it is important to reduce the consequences to human lives and critical infrastructure. Sacrificial sandwich panels which traditionally take the form of plate structure with a core layer encapsulated by face sheets on either side, are found to be efficient energy absorbents. As the sandwich structure deforms, energy is dissipated within the layers – reducing the forces transferred to other more critical components. It is important to understand the properties of the various panel layers and the interaction between them in order to optimise the energy absorption.

2. OBJECTIVES

The primary objective of the research project is to investigate, both experimentally and numerically, the mechanical behaviour of various sacrificial sandwich panel designs with core layer made out of aluminium foam materials.

3. A SHORT DESCRIPTION OF THE RESEARCH PROJECT

The main topics in the research project will be as follows:

1. The candidate conducts a study of relevant literature concerning sandwich panels and retrieve available experimental data of relevant materials.
2. Establish robust parameterised numerical models for sacrificial sandwich panels subjected to loading in the finite element code LS-Dyna in order to get an initial understanding of how key parameters influence the mechanical response of such designs.
3. The candidate shall conduct a numerical parameter study in order to investigate the effect of the chosen parameters on the energy absorption of the sandwich panels.
4. A series of experimental component tests with various sandwich design configurations shall be carried out in the SIMLab Shock Tube and Drop Tower to further the understanding of the underlying physical mechanisms in design characteristics and verify the results of the parameter study.
5. Finally, a comparison with existing results found in available literature is to be made.

Supervisors: Tore Børvik and Ole Vestrum

The candidate may agree with the supervisors to pay particular attention to specific parts of the investigation, or to include other aspects than those already mentioned. The thesis must be written according to current requirements and submitted to Department of Structural Engineering, NTNU, no later than June 10th, 2016.

NTNU, January 15th, 2016

Tore Børvik
Professor

Acknowledgements

Abstract

The main objective of this thesis is to conduct a numerical study of sacrificial sandwich panels with aluminium foam core. This is done in order to understand how different parameters affect the energy absorption when subjected to blast load and low-velocity impact. The sacrificial sandwich panels are made up of an aluminium foam core, and aluminium face sheets on each side. The face sheets have remained the same throughout the study, while the thickness and density of the foam core have been varied.

The Numerical models are established in LS-DYNA to replicate laboratory experiments in a drop tower and in the SIMLab ShockTube. Parametric studies were conducted to investigate the effect of varying foam core thickness and density. Laboratory experiments were conducted to validate the results of the parametric studies. The results of this validation showed that the blast loaded model replicated the correct trends, while there was larger problems with the model of the low-velocity impact.

Foam core sacrificial sandwich plates show good potential for absorbing energy from blast loads. Especially low-density foam shows potential for limiting the deformation while absorbing the energy. For low-velocity impact, further work is needed to conduct proper parametric studies, but experiments show promise of good results for low-density foam.

Contents

Chapter 1

Introduction

1.1 Background

The annual threat assessment for 2015, published by the Norwegian Police Security Service outlines a continued complex and varied threat picture to the Norwegian society with terrorist attacks as a possible threat [1], while The Norwegian Defence Estates Agency considers terror as a key part of the current threat situation, and points to protective structures as a key counter measure [2].

Based on this it is important to investigate the possibility of using new and innovative light-weight protection to secure sensitive and vital infrastructure. One possibility is to use sacrificial sandwich panels made of light-weight materials, like metallic of polymeric foams. This thesis will investigate the behaviour of sacrificial sandwich panels with aluminium foam core.

1.2 Energy Absorption in Protective Structures

The main objective of protective structures is to absorb the energy from the load, whether that is stopping a projectile or withstanding a blast [3]. This often happens through mechanical work, namely deformation and plastic dissipation. Therefore it is important to achieve as much plastic deformation as possible, within certain constraints such as failure, weight, displacement, etc.

There are different load situations that is relevant when designing protective structures. One is impact of projectiles. The aim of the structure would then be to stop the projectile before it perforates the target, preferable without ricochets or fragmentation [3].

Another situation is blast load, typically from explosions. This means the protective structure should absorb the energy of the propagating blast wave, without breaking and reflecting as little pressure as possible [4].

Since the aim is not simply to have a structure that can withstand the load, there are several ways to design protective structures. Cellular solids have a large potential for energy absorption, whether it is structured or unstructured cells, spanning over two dimensions, such as honeycombs or three dimensions like foams [5]. This has motivated several researchers to investigate these material's behaviour when subjected to blast and impact loads. For example, Zhu et al. [6] and Goel et al. [7] investigated the structural response of aluminium foam core sandwich panels subjected to blast loading. Other examples include Jang et al.'s [8] study of computational models for designing aluminium foam core sandwich panels, and Zhu et al.'s [9] optimal design study.

1.3   Objective

The objective of this study is to investigate the behaviour of aluminium foam core sandwich structures subjected to various blast and low-velocity impact loads, numerically and experimentally. Especially the energy absorbed in the structures will be investigated, and an optimal energy absorption will be pursued for varying density, thickness and weight.

The optimisation will happen through a numerical study to investigate the effect of varying the thickness and density of the foam core. Experimental studies will be conducted to assess the quality of the analyses, and relevance of the results.

1.4   Scope

The scope of this study is confined to the following:

- Material data will be taken from previous studies, and the Modified Johnson-Cook and Deshpande-Fleck material models will be used, as implemented in LS-DYNA [10].

- Analyses and optimisation will happen through modelling the test equipment available at SIMLab, namely the SIMLab ShockTube for blast load and a drop tower for the low-velocity impact.

- The thickness and material of the face sheets will be kept constant throughout the study.

- There will be a limited experimental study, mainly to validate the models used for the parametric study.

Chapter 2

Background

2.1 Material

The sandwich structures investigated in this study consist of two different materials, an aluminium alloy and aluminium foam. This section introduces the two materials and explains their properties and behaviour.

2.1.1 Aluminium

Aluminium is a light-weight metal. Due to its high specific strength, resistance to corrosion and flexibility to change its properties through processing, it is commonly used in structures where weight is important, such as automotive or aerospace applications [11].

Aluminium has a high ductility which makes it easy to form. In order to obtain higher strength it can be be alloyed, tempered or cold-worked, of which one or more is done for most aluminium in practical engineering applications [11]. This however usually decreases the natural corrosion resistance.

Norsk Standard, follows the European Standard and classifies aluminium in different series, depending on the alloy [12]. In different alloys are identified by a four digit number, where the first digit indicates the major alloy compound and the rest indicates the purity, [12]. The 1000 series is considered pure aluminium with an aluminium content of miniumum 99 % [13]. Finally, the tempering is given by a letter and a two-digit number. H indicates work-hardening [14].

The aluminium plates used in this study is 1050A-H14. Its material card can be found in Appendix A.1.

2.1.2 Aluminium Foam

Cellular solids are made up of an interconnected network of solid struts forming the edges and faces of the cells. Cellular solids can be two-dimensional, referred to as honeycombs, or three-dimensional, often called foams[5]. The number of dimensions refer to the packing of the cells. This gives a very light-weight material, and the single most characterising parameter is the relative density $\rho_r = \rho/\rho_s$, which is the density of the foam divided by the density of the cell wall solid [5].

A major division among foams is whether the cells are closed or open. In open-cell foam, the solid is contained only in the cell edges, and the cells connect through open faces. In closed-cell foam the cells are sealed off from each other. Aluminium foam is a cellular solid, where the cell walls are made up of aluminium, and the cells themselves are filled with fluid, usually air.

Goel et al. [7] mentions metal foam in particular as interesting for designing structures against mechanical impact and blast load. Wikipedia claims it was first reported in 1926, through a French patent [15]. There has later been several patents for manufacturing of metal foams, but commercial production only began in the 1990s, by Shinko Wire company in Japan [15]. Norsk Hydro also started producing aluminium foam around that time. The properties and potential caused a huge research interest to accurately describe its behaviour, and find applications for the new material. Especially the automotive industry was interested in its properties as light-weight energy absorbers, in studies such as [16], and [17]. In 2006 Hanssen et al [18] concluded that it would be possible to apply in car manufacturing with only a small weight gain, but it would complicate the manufacturing process and potentially increase the costs. This lead to researchers focusing on other usages, such as aerospace [19] and protective structures.

Technological advances has improved the usability of metallic foams, and this sparked new research interest, especially regarding its usage in protective structures against blast load [7]. An example of the research that proves alumnium foam's usage as an energy absorbes is Hanssen's study from 2002 [20], showing that the impulse transfer from a shock wave to a pendulum is larger when the pendulum is covered by an alumnium foam panel.

The deformation mechanisms of foam comes from three distinct contributions. For open-cell foam these are

- Cell-wall bending
- Cell-wal axial deformation
- Fluid flow between cells

For open-cell foams the two first can be described by idealising the foam cell as a cubic array of members, and applying beam theory to the deformation of these, as done by Gibson and Ashby [5]. Under compression the fluid is squeezed out, which means the viscosity of the fluid leads to a strong strain-dependence. Gibson and Ashby suggest that the simplest way to analyse this contribution is to treat the foam as a porous medium characterised by an absolute permeability, K.

For closed-cell foam the deformation comes from:
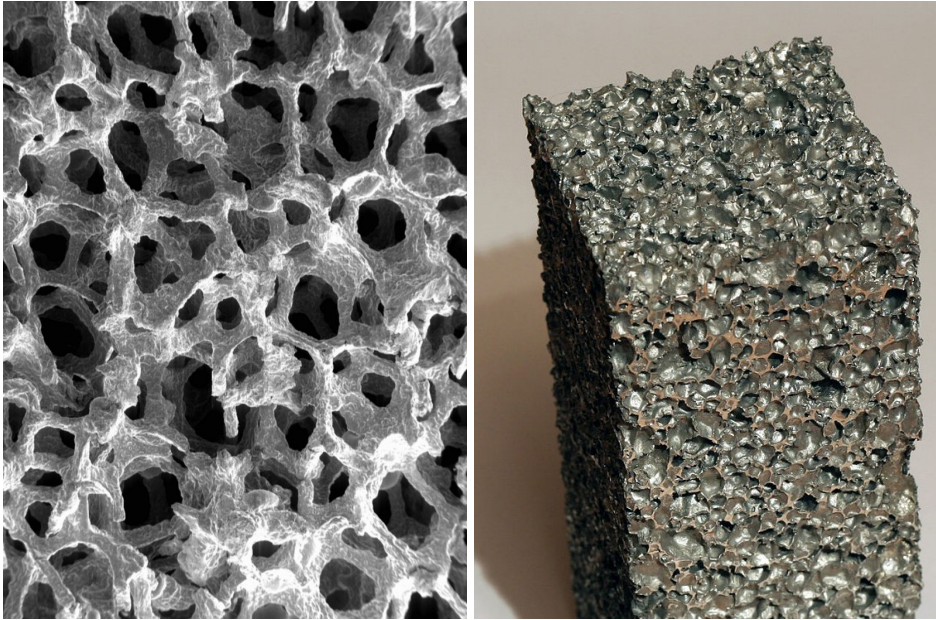
(a) [21]　　　　　　　　　　　　　(b) [22]

Figure 2.1: (a) Open-celled foam and (b) closed cell foam

- Cell-edge bending
- Edge contraction and membrane stretching
- Enclosed gas pressure

There is also bending stiffness in the cell faces, but as these are usually thin, especially in foams made from a liquid, these are rarely significant.

The enclosed pressure increases as the cells collapse, but as the pressure of the fluid inside the cells often is the atmospheric pressure, hence much smaller than the yield stress, this contribution is also often not important [5]. However, at high pressures this contribution would need to be taken into account.

These mechanisms cause the deformation of an elastic-plastic foam, which is a foam made out of an elastic-plastic solid to have three phases, explained by Gibson and Ashby[5] as :

1. Linear elasticity
2. Collapse plateau
3. Densification

The linear elastic phase lasts until the first cell-walls yields and collapses. Then there is a collapse plateau, where the cells collapse, before the solid reaches the densification phase as all the cells have collapsed, and the relative density approaches that of its parent
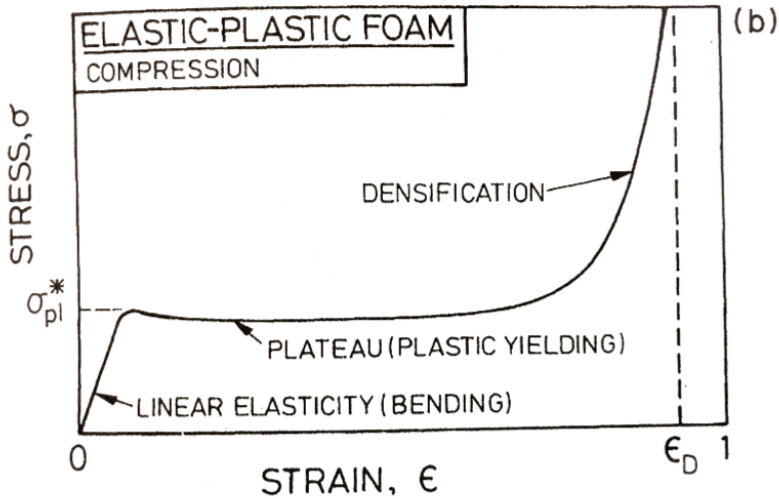
Figure 2.2: Typical deformation behaviour of cellular solids [5]

solid. Until the densification phase, this gives a deformation behaviour closely resembling an elastic-perfectly plastic behaviour, and allows for good load control and predictable deformation. This is a strong reason for the interest in applying cellular solids for energy absorption.

2.2 Sandwich Structures

Sandwich structures that consist of a light core covered by skins, are increasingly common in use, due to their high specific strength and stiffness [5] [23]. However, this is mostly true for internal structures as the damage resistance and tolerance is not extensively characterised [24]. Still the potential for sandwich structures as energy absorbers seem to have large potential, given the cellular solids, e.g. aluminium foam, show good energy absorbing properties. In 2015, Zhang showed that polymer sandwich panels, with thin faces absorbed more energy than similar panels with thicker faces [24].

2.3 Blast Loading

Blast load is usually coming from an explosion, where energy is rapidly released and a blast wave propagates out from the explosion due to inequilibrium between highly compressed air and the non-compressed surroundings [4]. The blast wave is characterised by an almost instantaneous rise, followed by an exponential decay. The decay usually leads to a phase
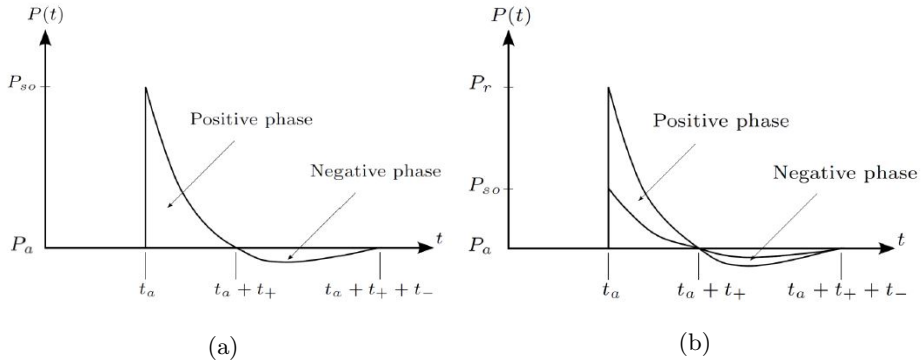
Figure 2.3: Characteristic pressure-time history for the (a) incident and (b) reflectedblast wave from an explosion [4]

where the pressure is lower than the ambient pressure, referred to as the negative phase. This usually lasts longer than the initial, positive phase, as illustrated in Figure 2.3a.

When the blast wave hits a structure it will be reflected with a larger magnitude. This reflected pressure wave will have a higher peak pressure than the incident wave, but apart from that the shape will resemble the former, as shown in Figure 2.3b.

There are several approaches to describe blast load in numerical simulations. A main difference between the approaches is how the Structure-Fluid Interaction (SFI) is modelled. The simplest way is to model the blast wave independantly of how the structure deforms. This way, the development of the pressure is set in advance. In order to obtain a realistic blast propagation, one can either numerically simulate the blast wave around the rigid structure, or one can use empirical methods.

A common empirical method to predict the blast wave's behaviour is through the Friedlander equation, which describes a exponential decay of pressure form the initial peak reflected pressure [4]. The equation is as follows,

$$P(t) = P_a + P_r \left(1 - \frac{t}{t_+}\right) exp\left(\frac{-bt}{t_+}\right) \tag{2.1}$$

where P_r is the peak reflected pressure, b is the exponential decay coefficient and t_+- is the duration of the positive phase. The reflected pressure is the actual loading on the structure.

Obviously, the blast wave is affected by the deformation of the structure. This can be described accurately by running a fully coupled Eulerian-Lagrangian simulation, simulating behaviour of both the structure and the fluid. However, this is a significantly more advanced simulation. In this study, only Lagrangian simulations have been conducted, with the blast load described by the Friedlander equation.

2.4 Equipment

Different kind of equipment has been used to conduct this study. The numerical analyses has been conducted in LS-DYNA, and the results from these, as well as the laboratory experiments have been post-processed in MATLAB. For the laboratory experiments other equipment has been utilised as well, most notably the SIMLAB ShockTube, an Instron drop tower and Digital Image Correlation. This section will explain this equipment.

2.4.1 Shock Tube

The experiments subjecting test specimens to blast loading in this study was conducted in the SIMLab ShockTube. The ShockTube is a good alternative to explosives in order to test structural response to blast load, as it enables load situations similar to explosions, but more predicatble, less hazardous and with fewer legal responsibilities [25]. The blast is launched by a sudden release of a high-pressure gas, generating a uniform shock wave propagating down the tube towards the test specimen. It creates a controllable and replicable shock wave as it depends on the initial conditions in the pressure chamber [25].

The ShockTube consists of a Driver Section and a Driven Section, divided by a Firing Section, as seen in Figure 2.4. The Firing Section is two pressure chambers divided by membranes. The Driver and Firing sections are filled with pressurised air. When the pressure reaches a certain value, the membranes break and sends a shock wave trough the Driven section. The amplitude of the shock wave can be determined by the strength of the membranes. [25]

To measure the pressure in the blast wave as it progresses, there are sensors place throughout the ShockTube. Particularly important to measure the impacting shock wave is the two sensors right in front of the test specimen. The position of these sensors are shown in Figure 2.4.
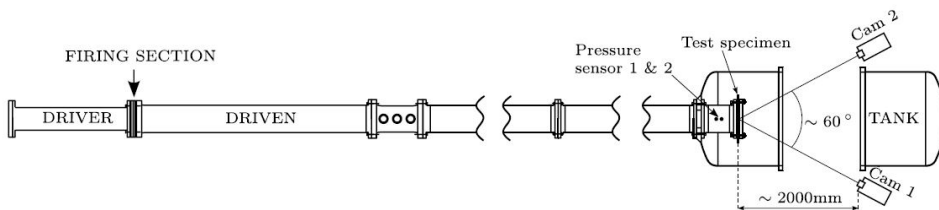

Figure 2.4: ShockTube Setup [25]

2.4.2 Drop Tower

The experiments subjecting test specimens to low-velocity impact in this study was conducted in an Instron CEAST 9350 Droptower Impact System, with an impact energy

capacity of 757 - 1800 J, and velocities ranging from 4.65 to 24.0 m/s.

An instrumented striker and striker-holder was used in order to obtain force data from the experiments. The force was measured by a load cell with a strain gauge, similar to Holmen's study [26]. Through Newton's second law and numerical integration one can obtain velocity and displacement data for the experiments, by use of Equation 2.2 and Equation 2.3:

$$v_{n+1} = v_n + \frac{F_{n+1} + F_n}{2m} \Delta t \tag{2.2}$$

$$d_{n+1} = d_n + (v_{n+1} + v_n) \Delta t \tag{2.3}$$

where F is the impact force and m is the total mass of the impactor, striker and striker-holder.
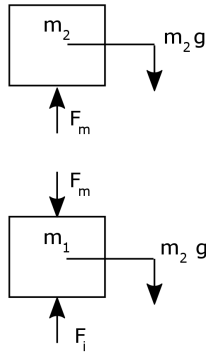
Figure 2.5: Force diagram of the striker, striker-holder and impactor of the drop tower

The force is measured behind the impactor. Figure 2.5 shows the forces on the impactor and on the striker and striker-holder, where, m_1 is the mass of the impactor, m_2 the mass of the striker and striker-holder, F_m the measured force and F_i the actual contact force. It is the impact force which is the impact force between the impactor and the sandwich panel that is of interest, and is used in calculation of the displacement. Through dynamic equilibrium for both parts of the impactor it is possible to establish the following equations:

$$\Sigma F_1 = m_1 a_1 = F_i - F_m - m_1 g \implies a_1 = \frac{F_i - F_m}{m_1} - g \tag{2.4}$$

$$\Sigma F_2 = m_2 a_2 = F_m - m_2 g \implies a_2 = \frac{F_m}{m_2} - g \tag{2.5}$$

As the acceleration is the same, it is means the impact force can be found from the measured force as

$$F_i = \frac{m_1 + m_2}{m_2} F_m \tag{2.6}$$

2.4.3   Digital Image Correlation

Digital Image Correlation (DIC) provides an opportunity to obtain displacement data throught-out an experiment, by analysing pictures from a high-speed camera. In its most basic form it works as a point-tracker, comparing subsequent images. More advanced one can obtain a displacement field through a global correlation through use of a Finite Element mesh [27]. Utilising two cameras, calibrated towards each other one can obtain three dimensional displacement. This makes the technique very useful for impact, blast and other transient experiments.

Chapter 3

Material

3.1 Aluminium Skin

The skins of the sandwich panels investigated in this study is made of low-strength and cold-rolled aluminium sheets, of alloy EN AW1050A-H14, produced by Norsk Hydro. Its material card can be found in Appendix A.1.

To describe and predict the material behaviour the thermoelastic-thermoviscoplastic constitutive relation proposed by Børvik et al. in 2001[28], has been used. This is based upon the constitutive relation and fracture strain model proposed by Johnson and Cook, as well as continuum damage mechanics proposed by Lemaitre, and includes linear thermoelasticity, the von Mises yield criterion, the associated flow rule, non-linear isotropic strain hardening, strain-rate hardening, temperature softening due to adiabatic heating, isotropic ductile damage and failure. The constitutive relation is defined as:

$$\sigma_{eq} = (1 - D) \left[\sigma_0 + \sum_{i=1}^{2} (1 - exp\,(-C_i p)) \right] [1 + \dot{p}^*]^C [1 - T^{*m}], \qquad (3.1)$$

where $\sigma_e q$ is the equivialent von Mises stress, p is the equivalent plastic strain, σ_0 is the yield stress and (Q_i, C_i, c, m) are material constant. The dimensionless plastic strain rate is given as $\dot{p}^* = \frac{\dot{p}}{\dot{p}_0}$, with $\dot{p}_0$ as a user-defined reference strain-rate. $T^* = \frac{(T-T_0)}{T_m-T_0}$ is the homologous temperature, where T_0 is room temperature and T_m is the melting temperature. The damage, D, follows the Cockcroft-Latham damage evolution rule [10]

$$\dot{D} = \frac{D_c}{W_c} \max\,(\sigma_1, 0)\,p, \qquad (3.2)$$

where D_c and W_c are material parameters

This model is highly suitable for impact and penetration problems, and is implemented in LS-DYNA as *MAT_107 [10].

The plates used in this study are the same as was described in Baglo and Dybvik's Master Thesis [29], and as the general trends are of higher interest than the exact results in this study, the material data is taken from their work.

3.2 Aluminium Foam

There are two sets of aluminium foam used in this study. The first set, which is used in the low-velocity impact analyses and drop tower experiments was produced by the continuous casting procedure patented by Hydro Aluminium AS, and is the same foam studied by Hanssen et al. when validating constitutive models for aluminium foam in 2002 [30] and by Reyes et al. when including fracture and statistical variation of density the year later [31]. Later they have been machined by Nomech to obtain the correct dimensions for this study.

The base material for the foam sheets are 8 % silica and 0.5 % magnesium balancing the aluminium (AlSi8Mg). The densities of the foam are supposedly between 0.1 and 0.5 g/cc, however this density has rather large variations.

The second set was Alusion Foam, delivered by CYMAT Technologies Ltd., delivered as finished plates. The two versions tested in the lab was AL-25.4-LG and AL-25.4-MD. Both were 25.4 mm thick panels with nominal densities of 0.17 g/cc and 0.33 g/cc, respectively.

3.2.1 Modelling of aluminium foam

There are in general two ways to model aluminium foam. One approach is two model it as a porous material, applying a constitutive model to the cell wall solid, and model the cells themselves. This is a very costly way of modelling, as it requires both generation of the cell structure and analysis of complex geometry.

A simpler way to model it is to model it as a continuum and mimic its behaviour through a constitutive model. In 2002 Hanssen et al. [30] compared several constitutive models for aluminium foam. Among the models investigated was Deshpande and Fleck's model from 2000 [32]. The result was that Deshpande and Fleck's model yields good results, but a fracture criterion was needed in order to obtain appropriate accuracy. The model is described by Reyes et al.[31] Given the yield function Φ is defined by

$$\Phi = \hat{\sigma} - Y \leq 0 \tag{3.3}$$

and the yield stress Y as

$$Y = \sigma_p + R(\hat{\epsilon}) \tag{3.4}$$

where $Y = \sigma_p + R(\hat{\epsilon})$ is the strain hardening and is the equivalent strain. Deshpande and Fleck [32] gives the equivalent stress $\hat{\sigma}$ as

$$\hat{\sigma}^2 = \frac{1}{[1 + (\alpha/3)^2]}[\sigma_e^2 + \alpha^2 \sigma_m^2] \tag{3.5}$$

where σ_e is the von Mises effective stress and σ_m is the mean stress. α defines the shape of the yield surface [31], and is given as

$$\alpha^2 = \frac{9}{2} \frac{(1 - 2\nu^P)}{(1 + \nu^P)} \tag{3.6}$$

where ν^P is the plastic coefficient of contraction.

In 2003, Reyes et al added fracture criteria, as well as randomly distribute density among elements to mimic variation in pore size [31]. The first fracture criterion was a strain-based criterion, initiating fracture when a certain strain level is reached. This means elements are eroded when Equation 3.7 is fulfilled.

$$\varepsilon_m \geq \varepsilon_{cr} \tag{3.7}$$

The second was an energy-based criterion, similar to Cockroft-Latham, as shown in Equation 3.8. The fracture criteria showed good results, while the distributed density gave little effect.

$$\int_0^{\hat{\varepsilon}} H(\sigma_1 - \sigma_{cr}) \sigma_{cr} d\hat{\varepsilon} \geq W \tag{3.8}$$

In this study the model proposed by Desphande and Fleck [32] is used, together with the strain based fracture criterion proposed by Reyes et al. [31]. This model is implemented in LS-DYNA as *MAT_154, and is chosen in this study for the combination of accuracy and simplicity. The energy-based fracture criterion is however not implemented. There is an option to add a stress-based criterion, eroding elements when Equation 3.9 is fulfilled for a certain number of cycles [10].

$$\sigma_1 \geq \sigma_{cr} \tag{3.9}$$

In his study in 2002, Hanssen conducted a large study of aluminium foam samples [30]. Based on the material tests, an equation for the density dependence of the Deshpande Fleck material parameters was constructed,

$$\sigma_p, \alpha_2, \gamma, 1/\beta = C_0 + C_1 (\frac{\rho_f}{\rho_{f0}})^n \tag{3.10}$$

where $\sigma_p, \alpha_2, \gamma$ and $1/\beta$ are parameters in the constitutive model, and C_0, C_1 and n, are fitting parameters. This allows to model aluminium foam of any density, and is therefore chosen in this study. The parameters' values are given in Table 3.1.

13

Table 3.1: Parameters of the Desphande Fleck model

	σ_p [MPa]	α_2 [MPa]	$1/\beta$	γ [MPa]
C_0 [MPa]	0	0	0.22	0
C_1 [MPa]	590	140	320	40
n	2.21	0.45	4.66	1.4

Young's Modulus, E, has been interpolated between the values used by Reyes in 2003 [31]. The interpolation is given by Equation 3.11. All parameters of the Deshpande Fleck model used in this study can be seen in Figure 3.1.

$$E(\rho) = 272.3081 + 58550\rho^{3.5704} \tag{3.11}$$

Research provides various results concerning the strain rate dependency of aluminium foam. Deshpande and Fleck [33] found no strain rate dependency. In 2016, Rajak et al conducted compression tests of aluminium foam and showed no specific relationsip between plateau stress and strain rate [34]. Therefore strain rate is not included in this study.

(a) E

(b) σ_0

(c) α_2

(d) β^{-1}

(e) γ
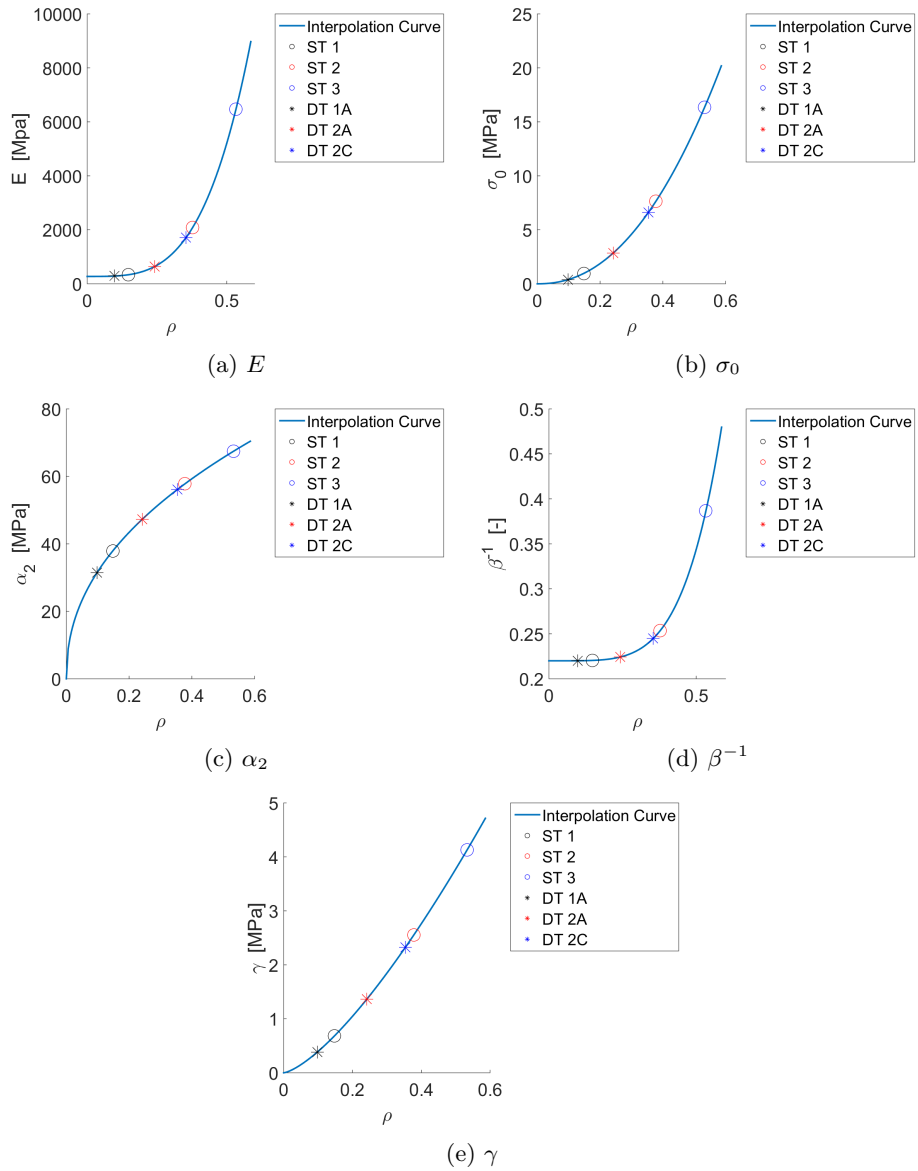
Figure 3.1: Parameters of Deshpande Fleck applied in this study

Chapter 4

Numerical Simulations

In order to accurately simulate the behaviour of the sandwich panels, a numerical model of the experiments was established. The model and all simulations have been conducted in LS-DYNA.

The material models were used as described in Chapter 3, both for the aluminium foam and the aluminium skins. Results of material tests were compared to Reyes [31], to ensure the model was correctly implemented.

4.1 Blast Loading

To assess the behaviour under blast loading, a numerical model similar to the experiment set-up in SIMLab ShockTube was established. The foam core was modelled with solid elements and the material was the Deshpande Fleck foam model, as described in Section 3.2. The thickness was initially set to 25.4 mm, though this was to be varied through parametric studies. The aluminium skins were modelled as shell plates with 0.8 mm thickness. The material was modelled as explained in Section 3.1, with parameters taken from the master thesis of Baglo and Dybvik [29]. For simplicity, the bolts were modelled as a linear elastic material and the support plates as a rigid material.

The contact algorithm used was the automatic surface-to-surface algorithm in LS-DYNA.

The boundary conditions were applied in the rigid plates, to ensure similar behaviour as in the physical experiment.

To keep the model simple and allow for multiple analyses with varying parameters, Structure Fluid Interaction (SFI) was not taken into account, and the blast load was modelled as pressure decaying like a Friedlander equation, see Section 2.3.
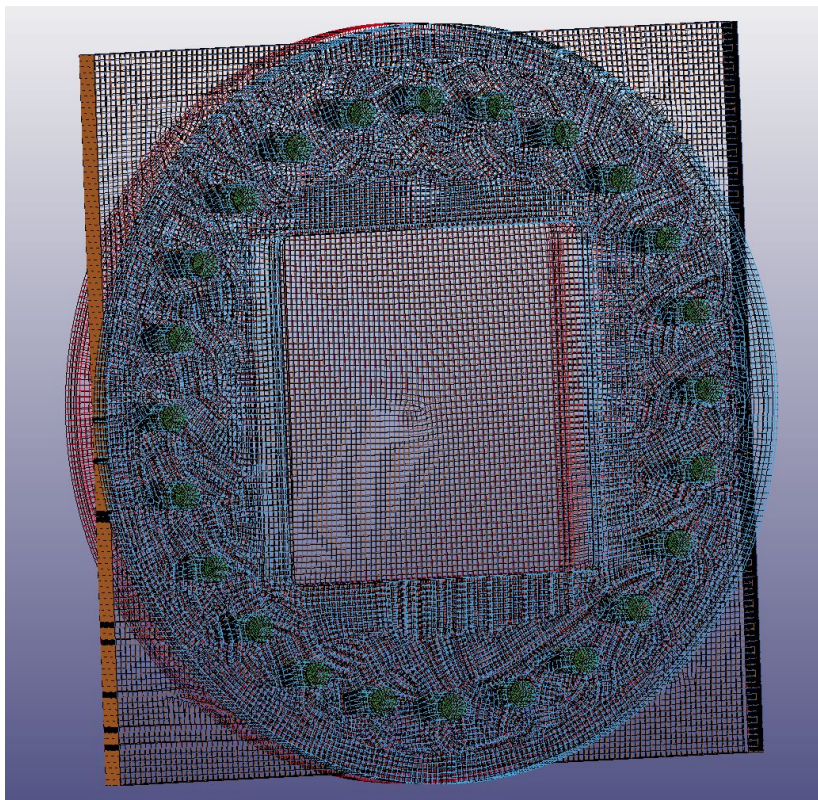
Figure 4.1: Numerical model for the blast load analyses

4.2 Low-Velocity Impact

To assess the behaviour under mechanical impact, simulations of a drop tower experiment was conducted. Due to symmetry, only one quarter of the panel, support and impactor was modelled.

The sandwich panel was modelled similarly to the model for blast load analyses, though the dimensions were 400 mm x 400 mm, and the core thickness was initially set to 50 mm.

As in the blast analyses, the boundary conditions were applied on the rigid plates, and the automatic surface-to-surface algorithm were applied. The bolts were modelled as linear-elastic, while the support and the impactor was rigid.

The load was applied through an initial velocity on a rigid impactor, which density was set in order for the mass of the impactor to be equal to the mass of the striker, striker-holder and impactor of the Drop Tower.
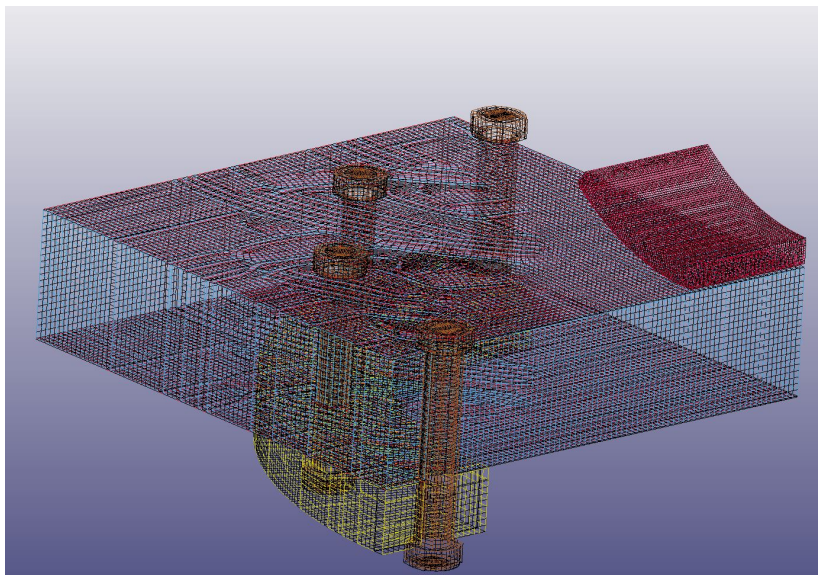
Figure 4.2: Numerical model for the low-velocity impact analyses

Chapter 5

Parametric Studies

To examine the effect of different parameters parametric studies as conducted. The varying parameters were the thickness and density of the foam core, as well as the load. These parameters were chosen as they are simple to adjust and makes it possible to compare with previous studies, e.g. Zhu et al. (2009) [9], Goel et al. (2015) [7] and Jang et al. (2015) [8].

5.1   Blast load

The aluminium skins have been kept the same through the study, while for the foam core, three thicknesses and three densities have been examined. The thicknesses were 12.7 mm, 25.4 mm and 50.8 mm, assigned as t_1, t_2 and t_3, respectively. Apart from the foam core thickness, the model described in Section 4.1 has been used.

Similarly, the three densities, 0.148 g/cc, 0.378 g/cc and 0.533 g/cc has been called ρ_1, ρ_2 and ρ_3. The material is modelled as explained in Chapter 3.

The blast load has been modelled by the Friedlander equation, described in Chapter 2.3, with constant b and t_d, while the peak pressures were $P_1 = 600\ kPa$, $P_2 = 900\ kPa$ and $P_3 = 1200\ kPa$.
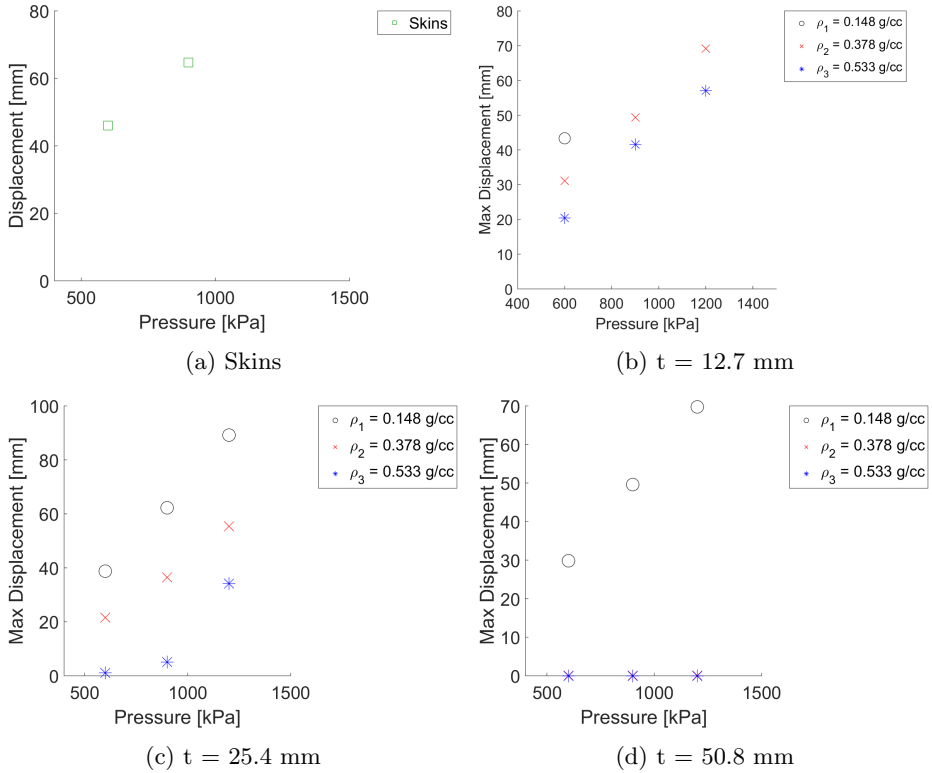
Figure 5.1: Maximum permanent displacement of the rear skin of sandwich panels of varying thickness

Figure 5.1 shows the mid-point deflection of the rear skin (the one opposite from the blast load), for the different thicknesses, densities and pressures. It is worth noting that this shows the applicable range of the parameters, in regards to load levels. The combination of t_1 and ρ_1 was not able to withstand pressures of 900 kPa and above. On the other side of the spectrum, t_3 did not undergo any deformation when subjected to the given pressures when the foam core was as dense as ρ_2 or denser.

From Figure 5.2, one can see a clear tendency for all thicknesses that the lower the density, the more energy is absorbed. Looking at Figure 5.1 it is evident that this coincides with the deformation of the whole sandwich panel, as a clear correlation between energy absorption and maximum displacement can be found.
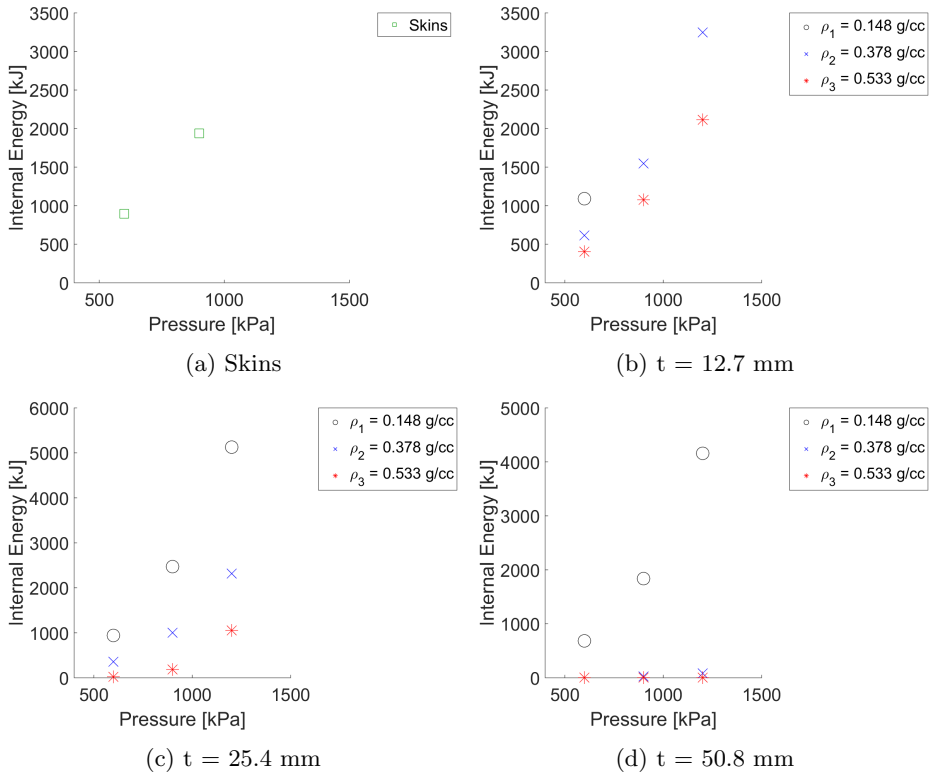
Figure 5.2: Total energy absorption in sandwich panels of varying thickness

In total the combination of smaller thickness and lower density yields higher energy absorption. This tendency holds until the sandwich panel can not withstand the pressure and fails, as was the case for t_1 and ρ_1 at $900 kPa$.

Not surprisingly the energy absorption per mass is also far larger for the thinner and lighter sandwich panels, as seen in Figure 5.3. Within each thickness, the lower-density foam clearly gives higher energy absorption per unit mass. Ultimately, the panels without a foam core, only two aluminium plates gives the highest specific energy absorption.
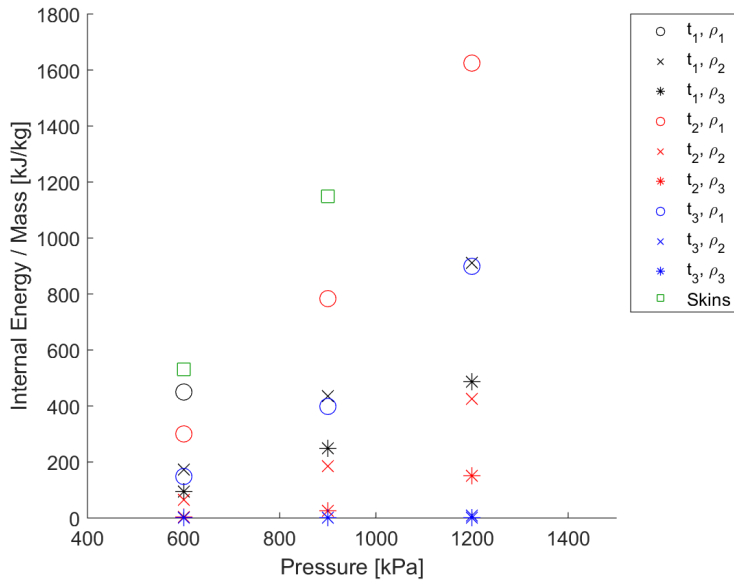
Figure 5.3: Total energy absorption normalised by total weight of the panels
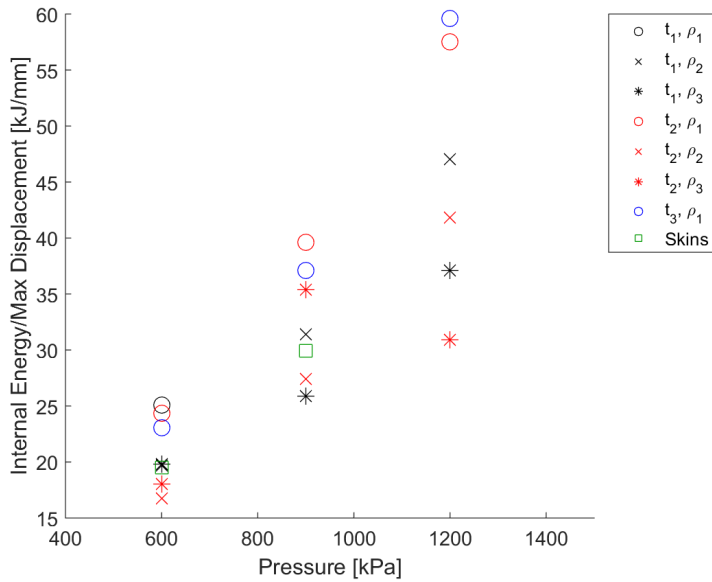
Figure 5.4: Total energy absorption per unit displacement

As the energy absorption so far has shown to be related to the deformation of the entire

plate, a way to look at the "efficiency" of the deformation with regards to energy absorption can be presented by the energy absorption per unit displacement, see Figure 5.4. Lower density of the foam, generally leads to higher energy absorption for each unit displacement. This might be caused by an increased amount of axial crushing of the foam cells, compared to plate bending in the entire panel. The low-density foam also yields higher energy absorption per unit displacement than the panel without foam core.
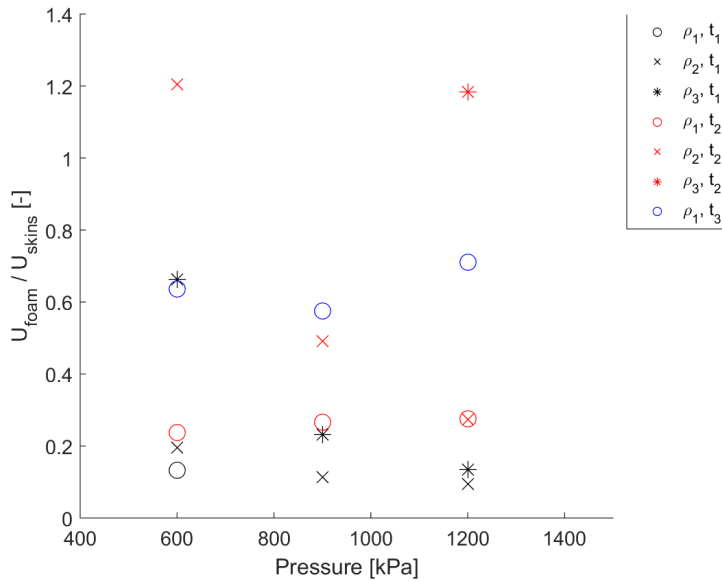
Figure 5.5: Proportion of energy absorbed by the foam core and the aluminium skins

To better understand the deformation modes, it is interesting to look at how the absorbed energy is divided between the foam and the skins. Figure 5.5 shows that for the denser foam at lower pressures a fairly high amount of the energy is absorbed by the foam core, while it decreases for higher pressures. For ρ_1 it ramains constant for a given thickness. ρ_1, t_1, is only included at 600 kPa, the panel did not withstand higher pressures. Similarly, t_3 is only represented with ρ_1, as Figure 5.2 shows it did not deform for denser foam.
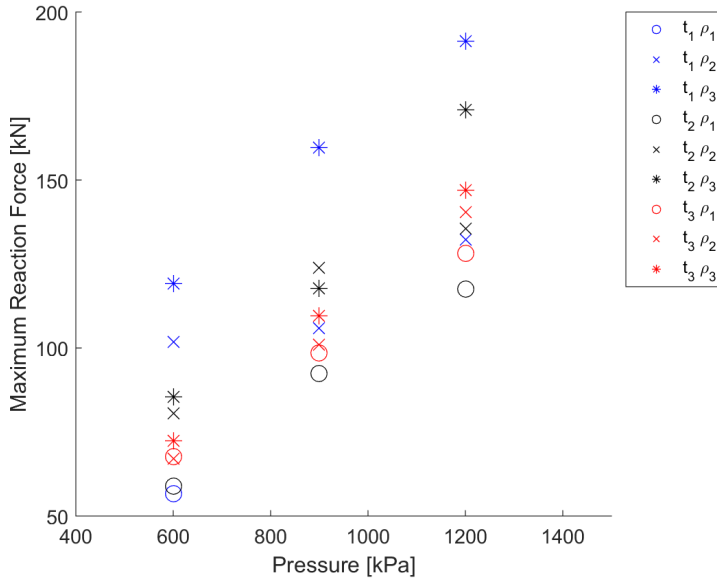
Figure 5.6: Maximum Reaction Force

When designing protective structures it is important to have knowledge on how the forces from the impact is transferred to the structure behind, in order to have the carrying structure strong enough to withstand the forces.Figure 5.6 shows the contact force between the rear plate and the support. One could expect the structures that undergo larger deformation, and thereby absorb more energy to transmit lower forces to its support, as more of the applied force goes to internal work of the structure. Therefore one can expect from Figure 5.2 that the reaction forces are lowest for the lighter density, and especially in combination with the smallest thickness.

Weight-equivalent Panels

To examine weight equvivalent sandiwch panels, the panels with $t_2 = 25.4mm$, were taken as reference and the corresponding thicknesses for other densities were calculated and shown in Table 5.1.

Mass [kg]	Density [g/cc]	Thickness [mm]
1.469	0.148	25.4
1.469	0.378	9.95
1.469	0.533	7.05
3.794	0.148	64.83
3.794	0.378	25.4
3.794	0.533	17.99
5.293	0.148	91.51
5.293	0.378	35.86
5.293	0.533	25.4

Table 5.1: Parameters of the Weight-Equivalent Panels

Figure 5.7 shows again that the energy absorption is higher for lower densities. It is however worth noting that when looking at the normalised energy absorption in Figure 5.8, the most important parameter is the weight of the sandwich panel, as all the panels of the lowest mass m_1 has highest energy absorption. Among the plates of the same weight however, those with the lowest core density has the highest specific energy absorption.
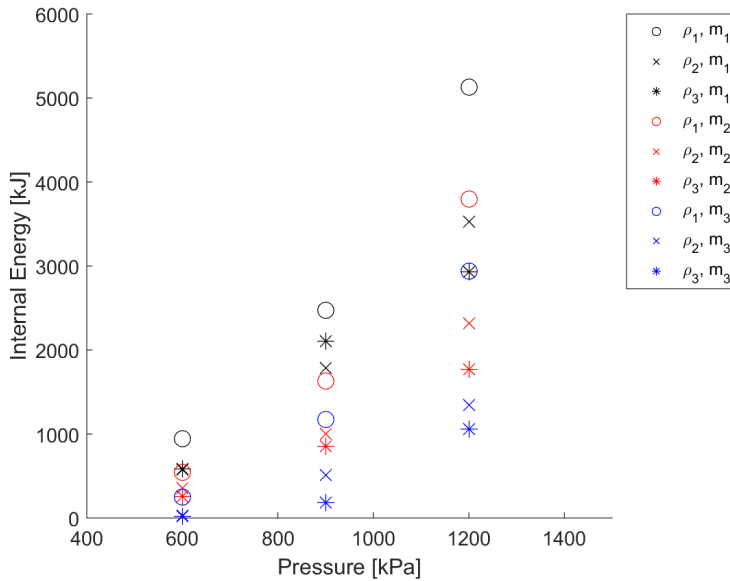
Figure 5.7: Energy absorption
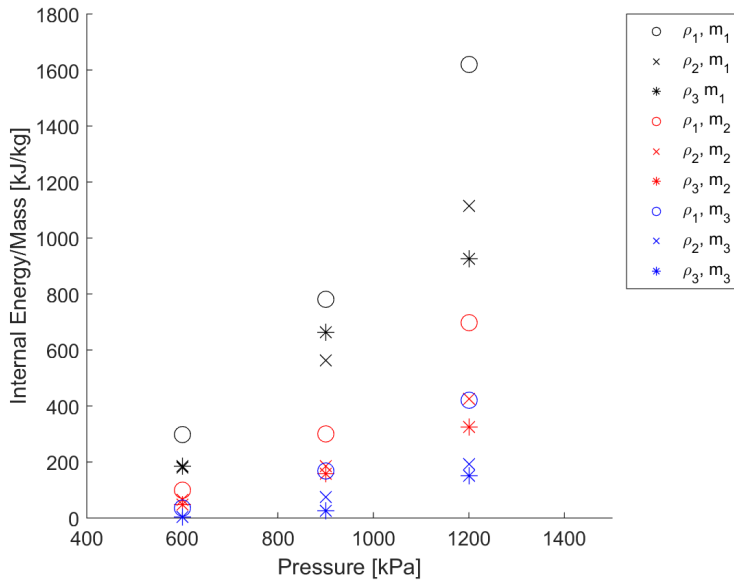
Figure 5.8: Energy absorption normalised by weight

When the displacement is a priority, the density is the most decisive, as Figure 5.9 shows. However, the thin plate with ρ_3 core, shows large energy absorption compared to the displacement.
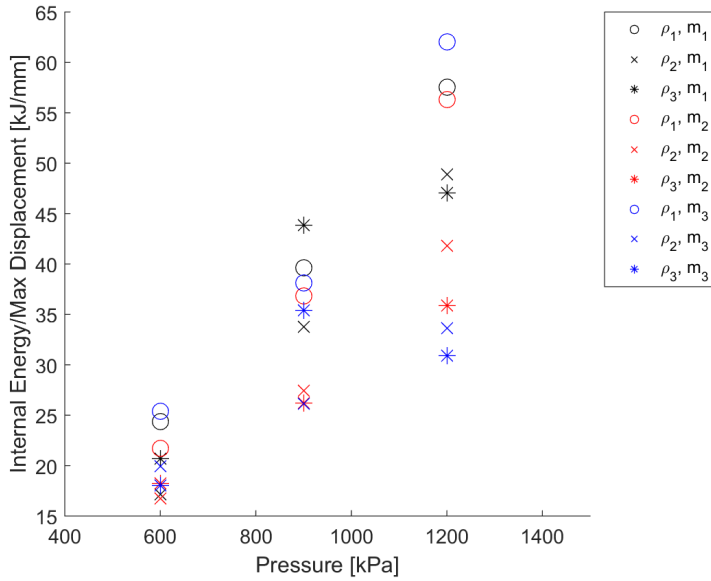
Figure 5.9: Energy absorption per unit displacement

5.2 Low-velocity Impact

The model described in Section 4.2 has been used. Three densities, 0.098 g/cc, 0.242 g/cc and 0.354 g/cc, have been examined. They have been called ρ_1, ρ_2 and ρ_3. The aluminium skins have been kept the same throughout the study. The materials have been modelled as explained in Chapter 3.
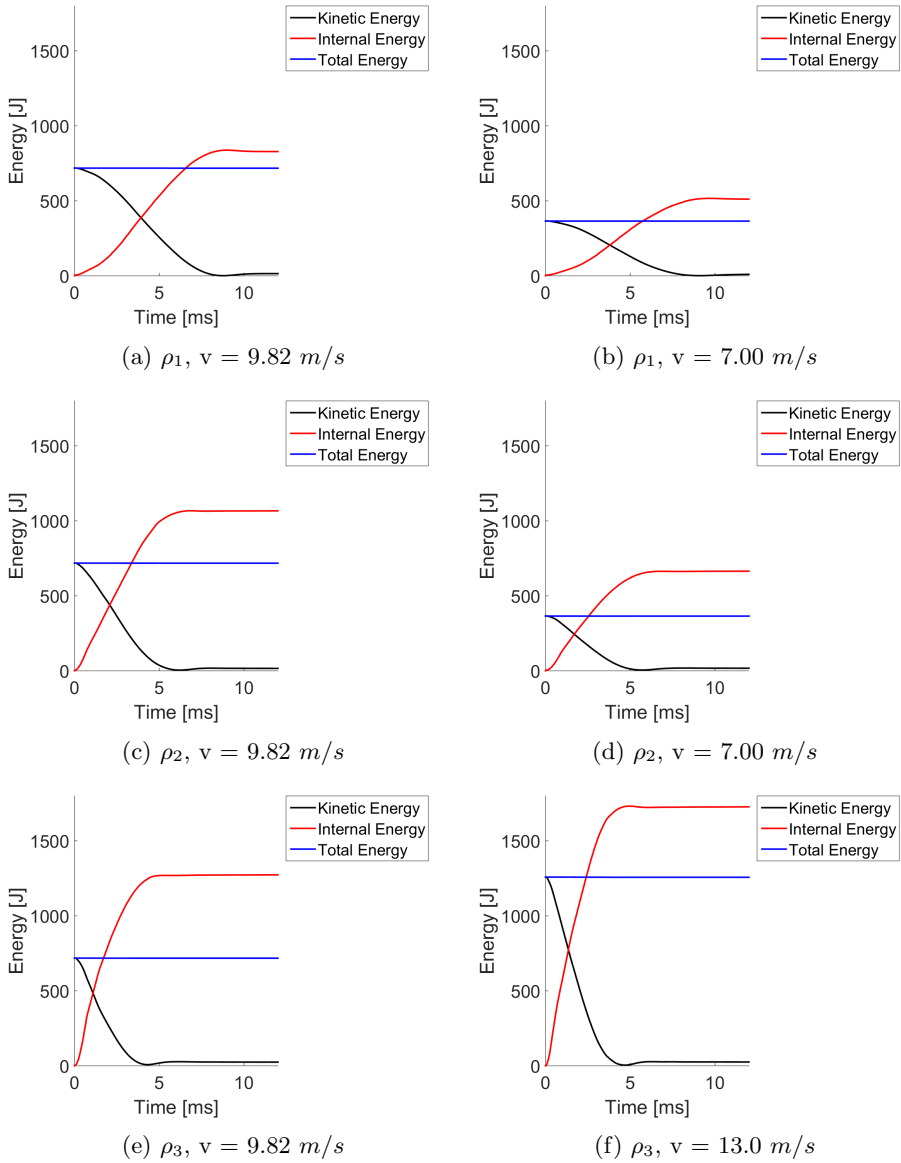
Figure 5.10: Energy levels in the analyses in the parametric study of low-velocity impact

In the analyses of the low-velocity impact a problem in the contact formulation between the skins and the foam core, causing a negative contact energy, was obtained just before the deadline for this thesis. Figure 5.10 shows that the final internal energy is higher than the initial kinetic energy, with an increasing difference as the density increases.

Figure 5.11 indicates that the energy absorption is higher when the foam core is denser.

This is opposite of the trend from the parametric studies on th blast loaded panels, and also opposite of the results from the experiments in Section 6.2. This might be caused by the artificially high internal energy seen in Figure 5.10 as difference is higher for higher densities, overshadowing a possible opposite trend similar to that of the blast loaded panels.
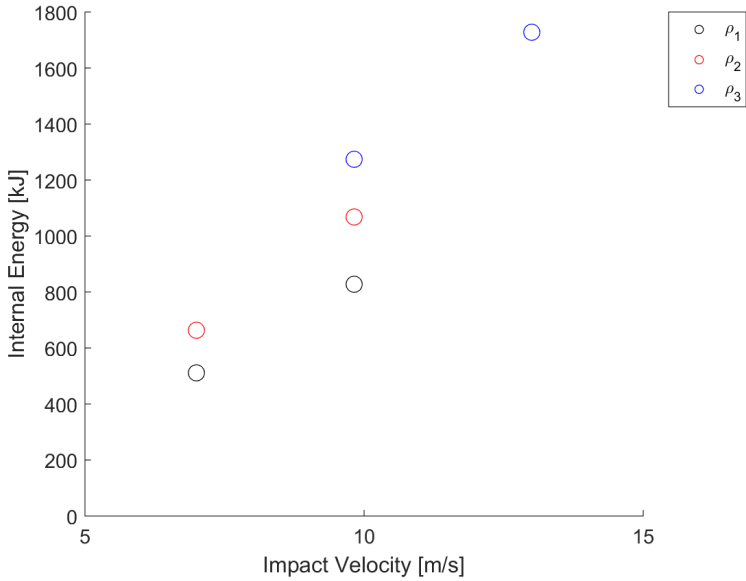
Figure 5.11: Energy absorption in

The displacement from the analyses is closer to what could be expected. As the density of the foam core increases, the maximum displacement of the bottom skin decreases, as shown in Figure 5.12.
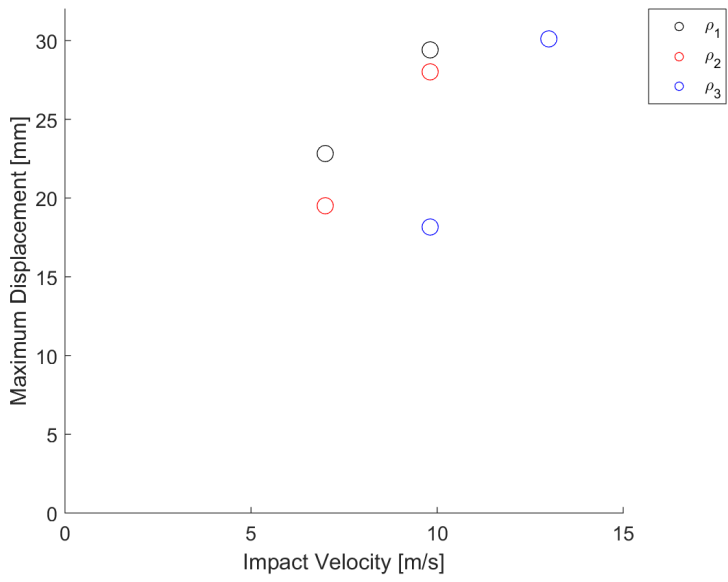
Figure 5.12: Maximum Displacement

Chapter 6

Experiments and Validation

In order to assess the quality and reliability of the numerical analyses, and to verify the results from these, experiments were conducted for both blast load and low-velocity impact.

6.1 Blast Load

6.1.1 Test Setup

The aluminium foam plates had nominal dimensions of 625x625x25.4 mm, and given density of 0.17, 0.33 and 0.51 g/cc, respectively.

The foam plates were weighed. The results are shown in Table 6.1. Note that it is a very small sample, and rather large variations. The densities have been calculated based on the nominal dimensions. For the analysis conducted in this study, the measured densities have been used.

The plates were fastened using M24 bolts, and tightened with a 10 Nm torque wrench. There was an aluminium skin of thickness 0.8 mm on each side of the foam core. The aluminium skins were 1050A-H14, as described in Subsection 2.1.1.

Table 6.1: Results of measurement of the aluminium foam plates

Nominal density $[g/cc]$	Weight $[g]$					Average weight $[g]$	Measured density $[g/cc]$
0.17	1429	1443	1500	1499	1474	1469	0.148
0.33	3809	3749	3717	3765	3796	3749.2	0.378
0.51	5205	5428	5317	5297	5216	5292.6	0.533
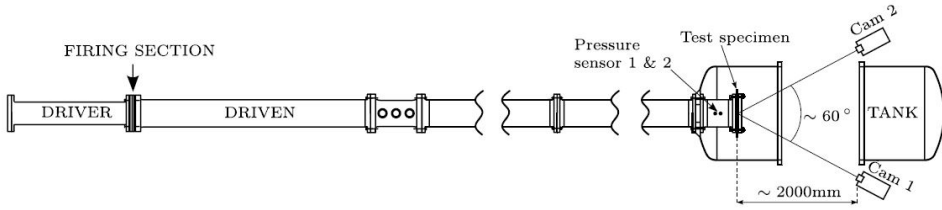
Figure 6.1: ShockTube Setup [25]

Table 6.2: Test programme of the ShockTube experiments

Test	Driving Pressure [bar]	Foam Density [kPa]	[g/cc]
P10 2A	10	0.148	
P10 3A	10	0.378	
P10 Skins	10	-	
P15 2B	15	0.148	
P15 3B	15	0.378	
P15 Skins	15	-	

The pressure was measured by two sensors shown in Figure 6.1. To capture the structural response of the plates, two Phantom v1610 High-Speed Cameras were used to gather input for a DIC analysis.

Panels of two different foam densities were tested at two different pressures. The aluminium skins were also tested without a foam core, at the same to pressures. The tests conducted in the ShockTube can be seen in Table 6.2.

6.1.2 Pressure Calibration

The tests were conducted at two different pressures. The pressures in the driving sections were 10 and 15 bar respectively. The pressures measurements can be seen in Figure 6.2.

As explained in Chapter 2.3, the pressure was calibrated against the Friedlander equation in order to obtain input for the numerical models. The resulting graphs can be seen plotted against the pressure measurements in Figure 6.3, and the parameters used as input for the numerical analyses are shown in Table 6.3.

As the P15 Skins experiment ended with completely tearing, the reflected pressure wave is not representative of the actual load. For the validation of the model at this pressure, the data from P15 3B will be used.
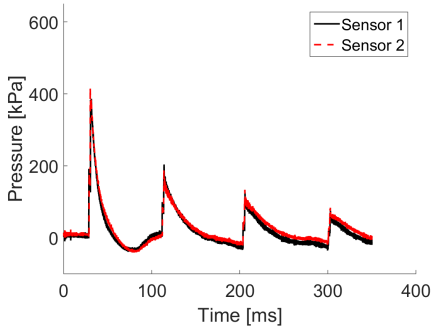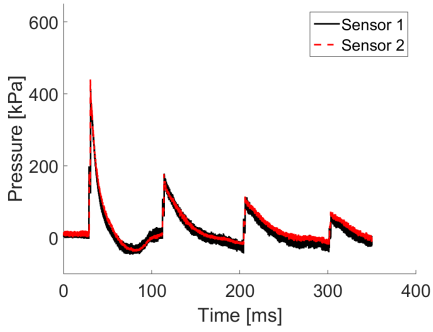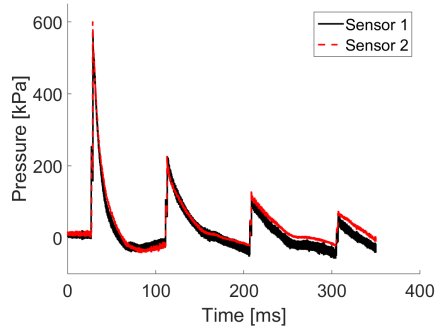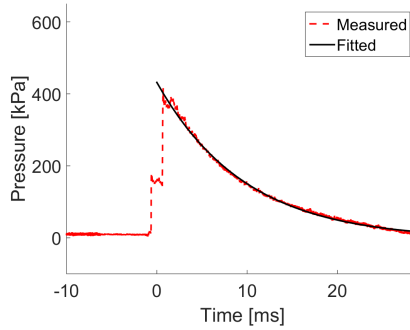
(a) P10 Skins
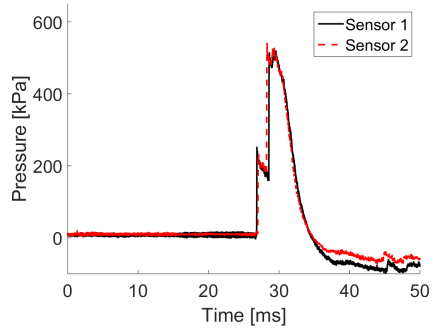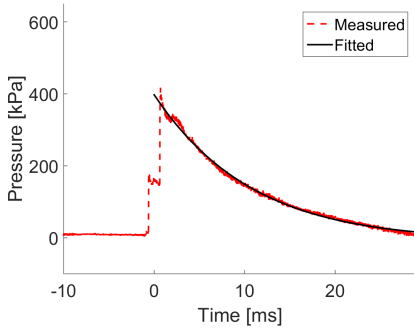
(b) P15 Skins
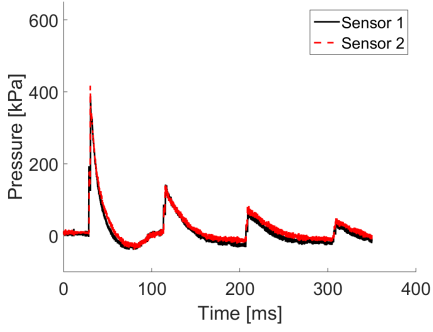
(c) P10 2A
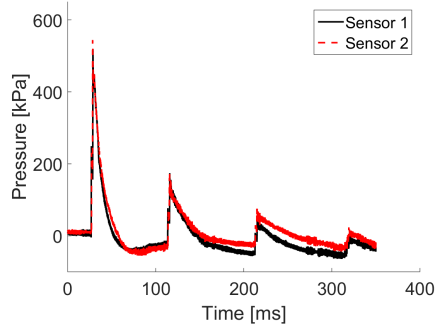
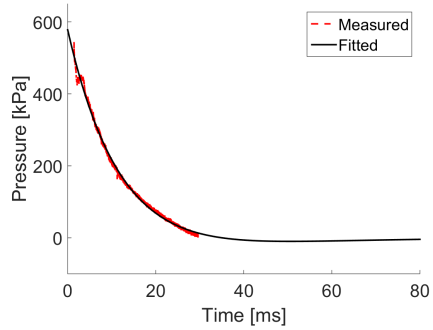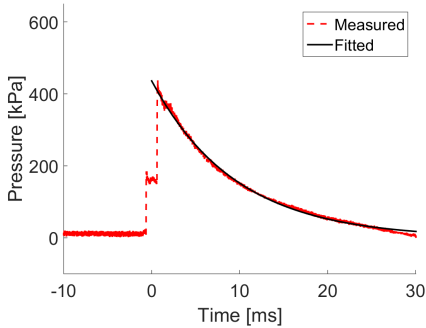(d) P15 2B

(e) P10 3A

(f) P15 3B
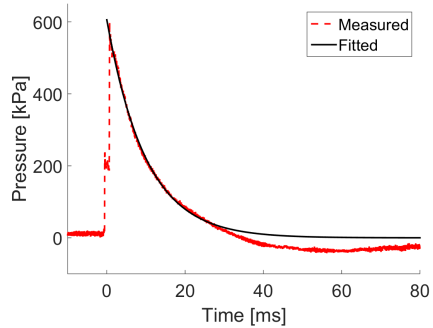
Figure 6.2: Pressure Measurements

(a) P10 Skins

(b) P10 2A

(c) P15 2B

(d) P10 3A

(e) P15 3B

Figure 6.3: Pressure Measurements fitted to Friedlander Equation

6.1.3 Results and Verification

Looking at the pictures of the experiments in Figures 6.4 through 6.9, it is obvious that the foam core brings additional strength to the panels, as the two layers of skins completely

Table 6.3: Parameters of the fitted Friedlander Equations

Test	Driving Pressure [bar]	P_r [kPa]	t_d [ms]	b [−]
P10 2A	10	397	42.9	3.072
P10 3A	10	436	10.47	9.99
P10 Skins	10	432	52.7	4.46
P15 2B	15	578	35.05	2.25
P15 3B	15	606	109.4	9.99

teared by the support when subjected to the blast from the 15 bar driving pressure, as seen in Figure 6.5. Moreover, the lighter foam experienced larger deformation than the denser foam at both pressures.

Since the exact results are of lower interest than the general trends in this study, the experiments and analyses will be compared only by the visible deformation and maximum displacement.
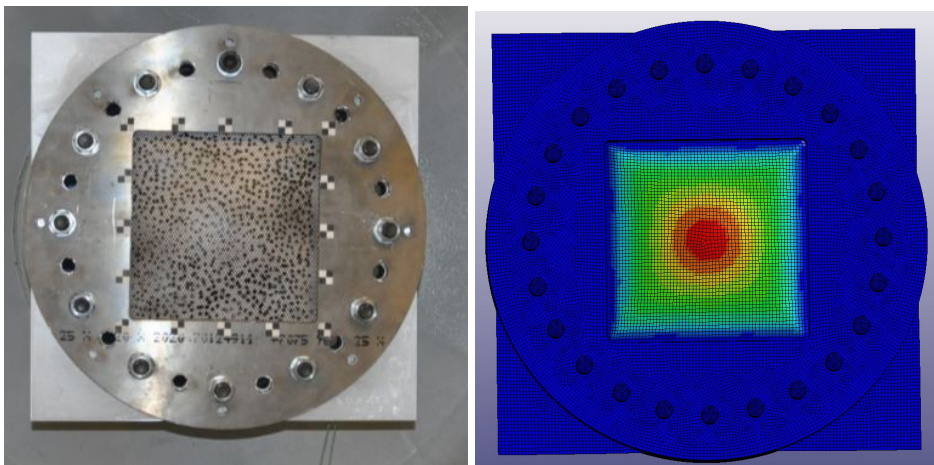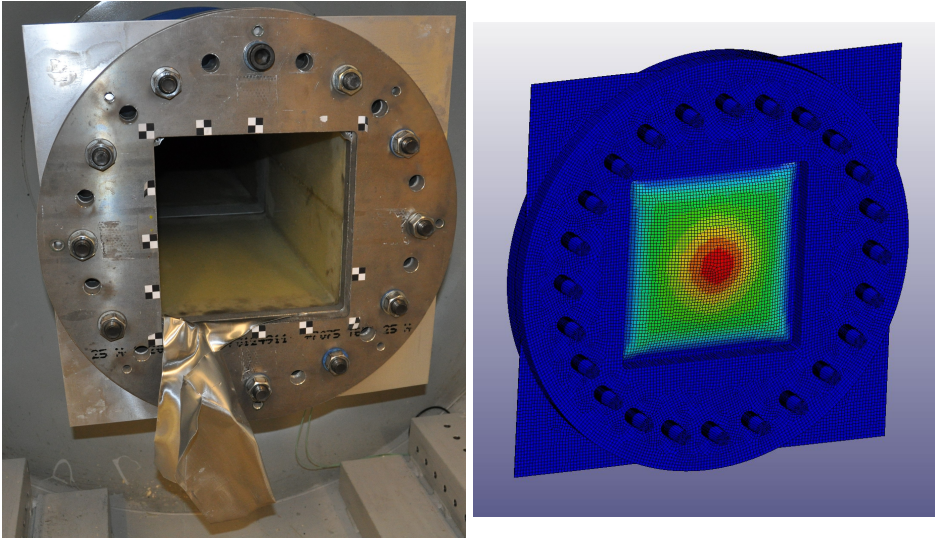

Figure 6.4: P10 Skins

Figure 6.5: P15 Skins

Figure 6.4 shows that the deformation of the skin when subjected to the blast from a driver pressure of 10 bar, is replicated rather well. However, Figure 6.5 clearly shows that the failure criterion is not accurate. In the analysis, failure is not initated, while there is complete tearing along the support in the experiment.
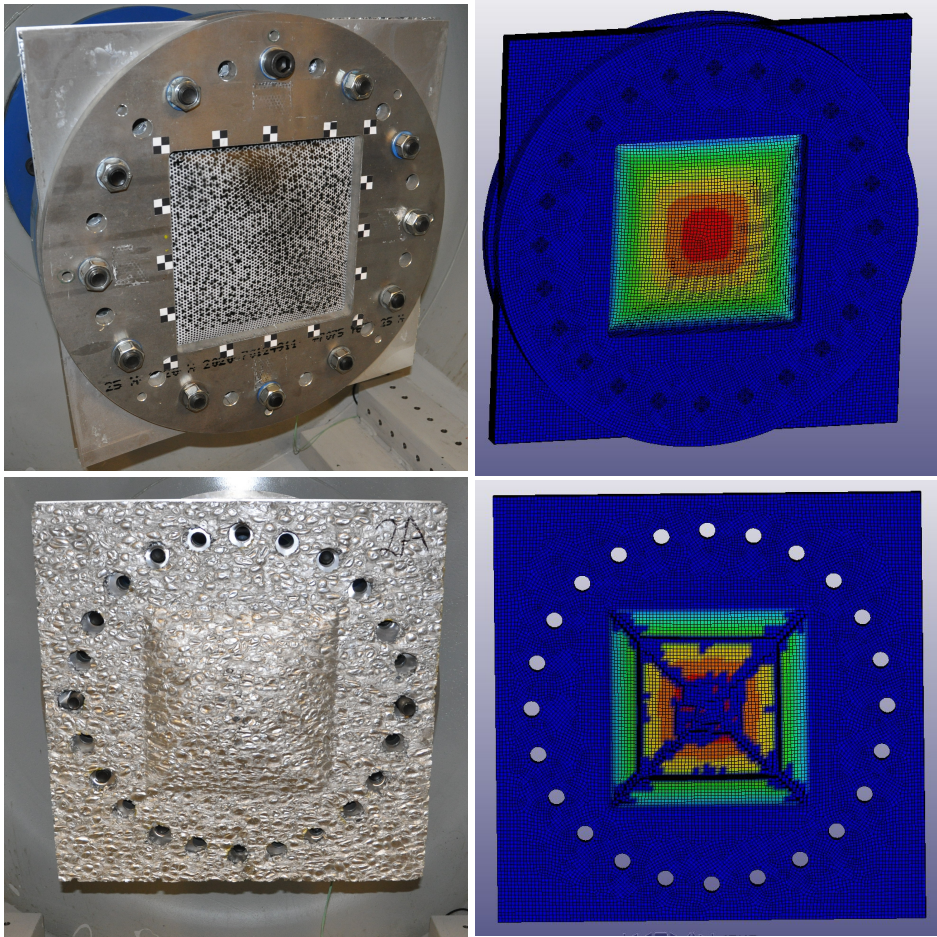
Figure 6.6: P10 2A

Figure 6.6 shows little visible fracture in the foam core, and a smooth displacement of the rear skin. The analysis seem to overestimate the fracture in the foam.
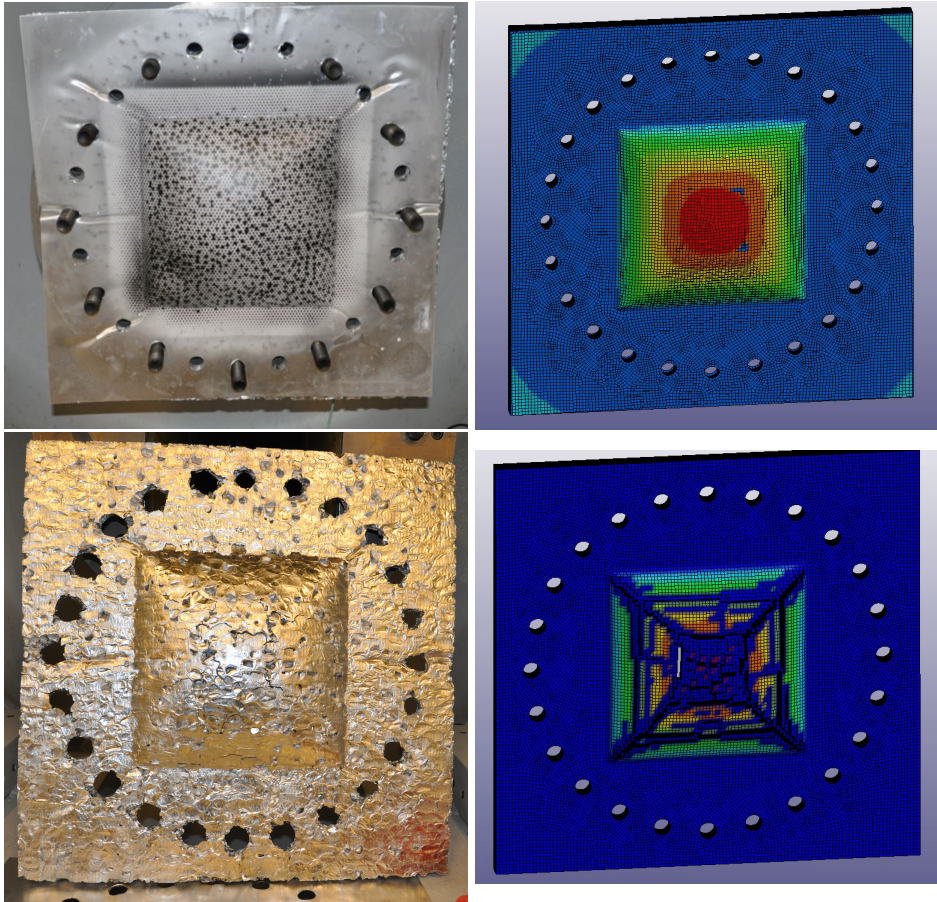
Figure 6.7: P15 2B

Figure 6.7 shows that there is more deformation, than in the previous test, and also more fracture of the foam core. There is a slightly visibly X-shaped fracture pattern in the laboratory test, which is clearly shown in the analysis, as it again seem to overestimate the foam fracture.
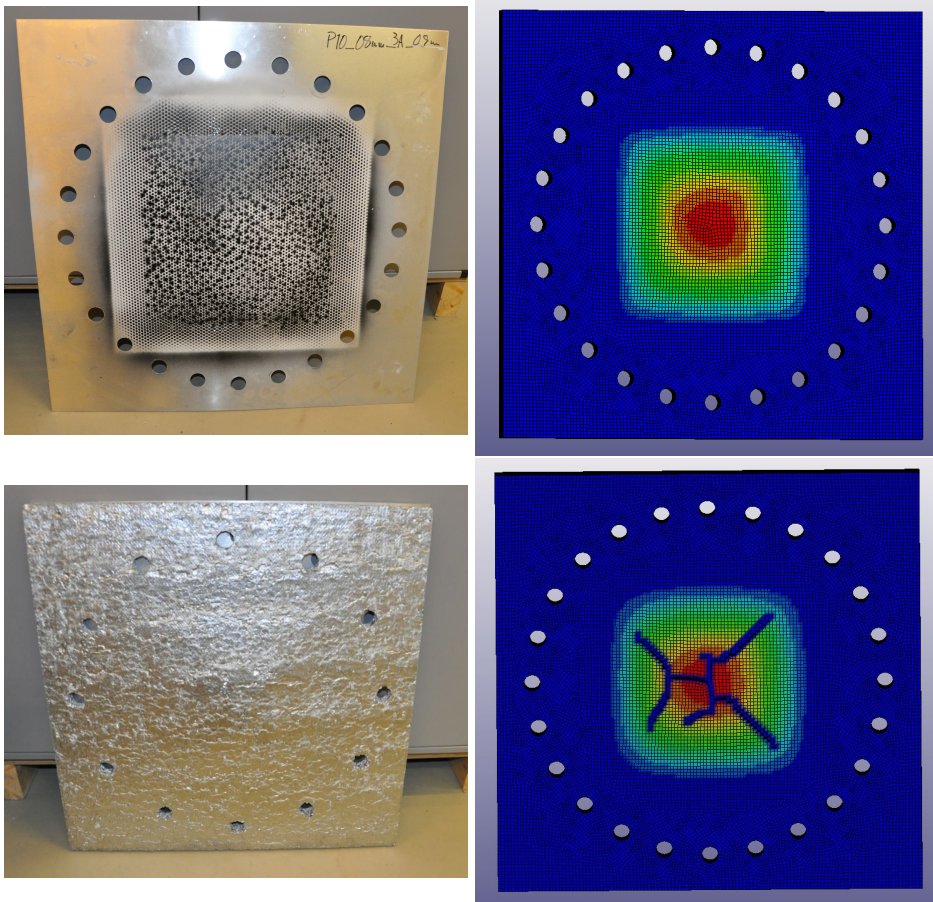
Figure 6.8: P10 3A

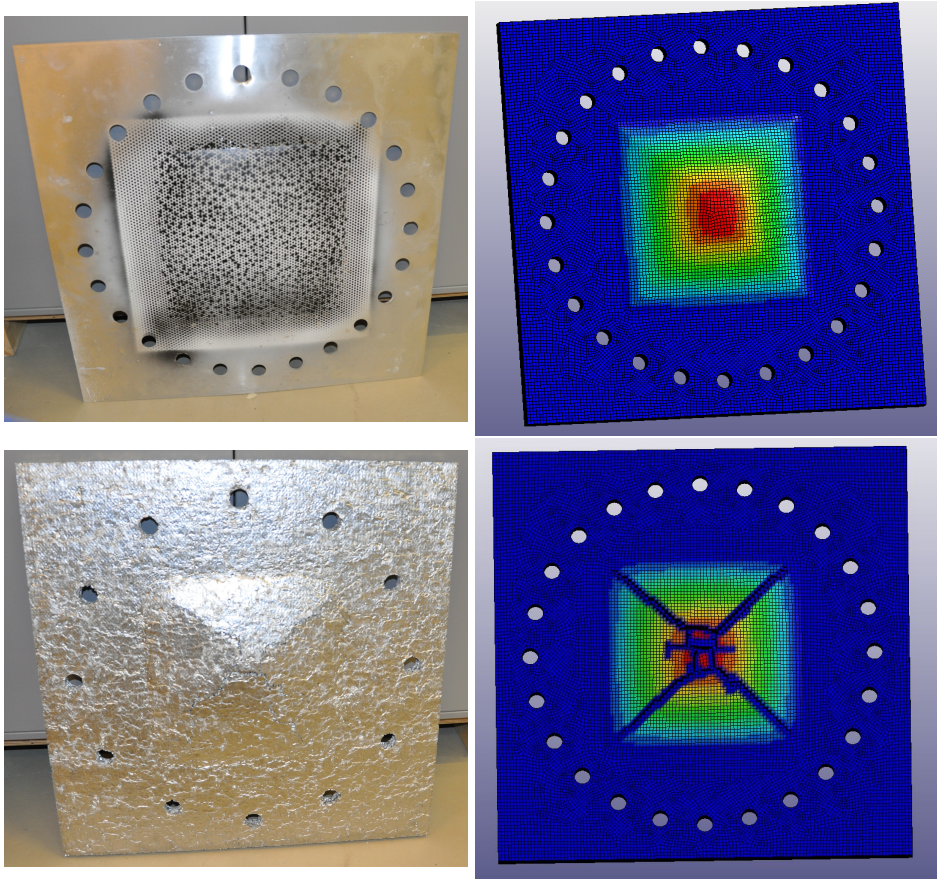Figure 6.8 shows less deformation than the two previous panels, and also little fracture.

Figure 6.9: P15 3B

Figure 6.9 shows a different deformation shape than previous tests, with a clear X-shaped fracture and an almost pyramidic deformation of the foam. The X-shape fracture pattern is clarly visible in the analysis.

In Figures 6.6, 6.7, 6.8 and 6.9, one can see similar deformation modes occuring in both analyses and experiments, though the analyses tend to overestimate the amount of failure in the foam.

Looking at Figure 6.10, on can see that the analyses of the foam panels show smaller displacement than the experiments, while the analysis of the double aluminium skin without foam overestimates the displacement. This might be caused by premature erosion of the foam elements, and therefore less energy absorption. However, the analyses capture the same trend of larger displacement for lower density, as one could find in the experiments.
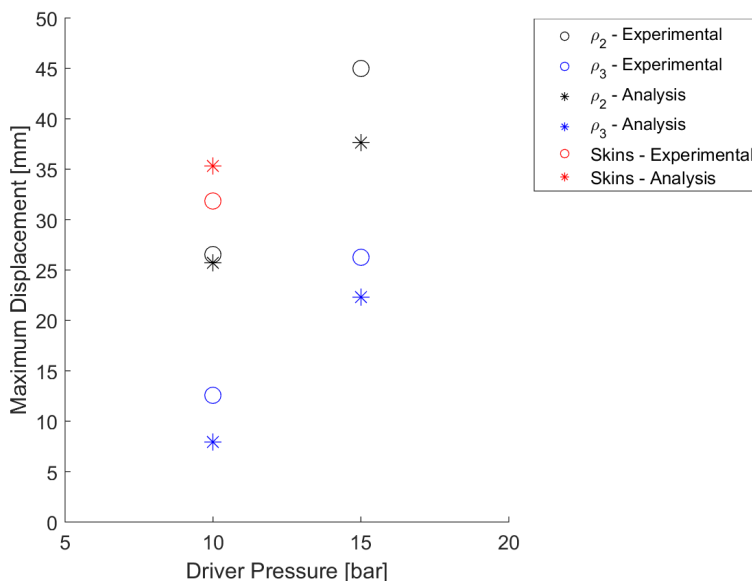
Figure 6.10: Comparision of analyses and experiments

6.2 Low-velocity Impact

6.2.1 Test Setup

The aluminium foam plates were machined to have nominal dimensions of 400x400x50 mm. The test specimens were assumed to have two different densities, as stated by Tømte [35]. The two assumed densites will be called Density Series 1 and 2. The foam plates were measured and weighed. The results can be found in Table 6.4. It is clearly a wide variety in the densities. Still the plates in Series 2, seems to be two distinct ranges of densities one around 0.25 g/cc and one around 0. 37 g/cc. This is in agreement with the results from Hanssen's study in 2001 [30], where they operated with three groups of densities. However, the values of the densities are not similar to his results. The lowest density was measured to be around only 0.098 g/cc, meaning it is outside the range of the interpolation Hanssen made. In this study, the parameters for the foam of the lowest density has been extrapolated, using the same equations.

The machining of the foam plates were done by Nomek. Test 2D revealed that there was water in the foam, when it flowed out through a tiny crack shown in Figure 6.20. This was probably cooling water. The presence of the water within the cell structure, will affect the behaviour as the foam, as there is viscous effects in the cells, as discussed in Section 3.2. These effects have been neglected in this study. The influence this might have on the results will be discussed in Chapter 7. The water in the foam pores will also have lead to an overestimation of the density of the foam, which is also not accounted

for. The additional weight from the water might explain the deviation from Tømte's [35] measurements.

Figure 6.11 shows a machining flaw in the foam. This was not taken into account in analyses later, as it is believed to not contribute significantly to the panels integrity.

Figure 6.11: Flaw in test specimen 2A

Table 6.4: Test Specimens for the drop tower experiment

Density series	Test Specimen	Weight [g]	Width [mm]	Height [mm]	Thickness [mm]	Density [g/cc]	Relative Density [%]
1	A	775.7	397	399	50	0.0979	3.6
1	B	780.4	398	399	50	0.0983	3.6
1	C	740.5	400	399	49	0.0947	3.5
1	D	733.0	399	397	50	0.0925	3.4
2	A	1849.3	399	399	48	0.2420	9.0
2	B	2090.4	400	400	50	0.2613	9.7
2	C	2820.9	399	399	50	0.3544	13.1
2	D	3043.8	399	398	49	0.3912	14.5

The tests were conducted in an Instron CEAST 9350 Drop Tower, as described in Subsection 2.4.2. The aluminium foam core was mounted with aluminium skins on each side and fastened by 12 M24 bolt to a circular frame, as shown in Figure 6.12. The bolts were not tightened, in order to avoid additional clamping, only support and ensuring that the test specimens would be kept in place.

The mass of the impactor was 14.985 kg, and the test velocities are shown in Table 6.5.

Table 6.5: Test Setup of Drop Tower Experiments

Test	Core [g/cc]	Impact Velocity [m/s]
S1	-	4.77
S2	-	6.82
S3	-	9.84
1A	0.0979	9.82
1B	0.0983	6.8
1C	0.0947	9.86
1D	0.0925	6.81
2A	0.2420	9.84
2B	0.2613	6.82
2C	0.3544	9.82
2D	0.3912	12.79

Figure 6.12: Test set up for the drop tower experiments

6.2.2 Experimental Results

Test specimen 1A showed significant compression of the foam core, and strong deformation of the top skin. The top skin tore along the sharp edge of the impactor. There was no failure in the bottom skin, and the deformation was smooth.
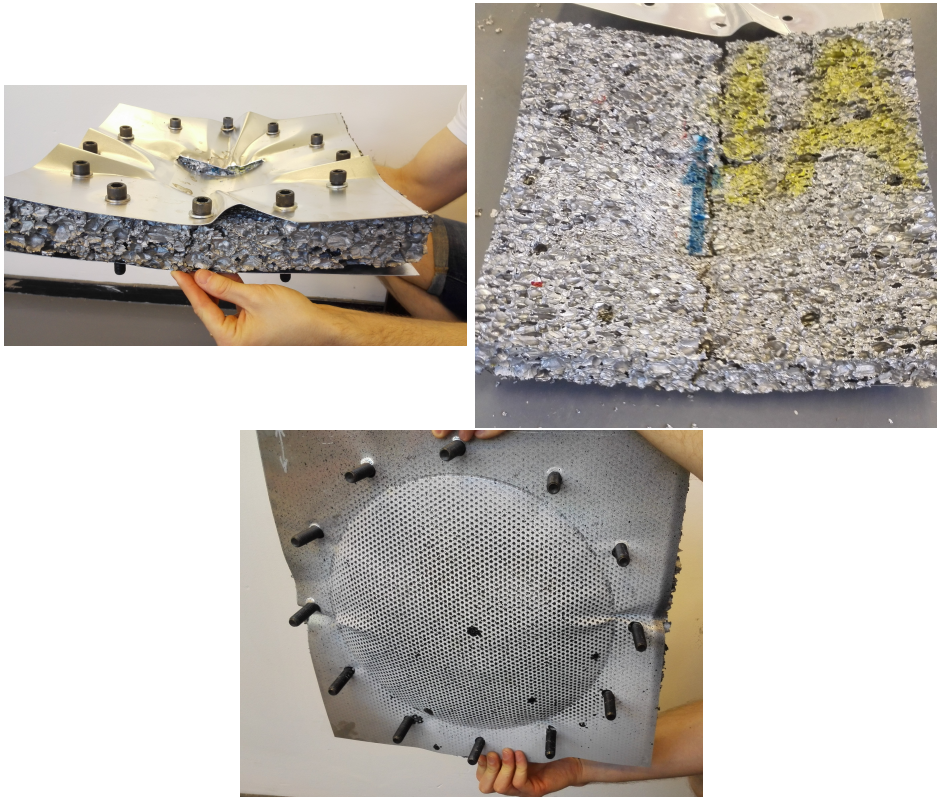
Figure 6.13: Test 1A

Also in test 1B did the foam compress, especially right beneath where the impactor struck. The top skin have buckled around the bolts, and tore along the sharp edge of the impactor. The bottom skin was not fractured.

Figure 6.14: Test 1B

Test 1C showed similar deformation as 1A, but the fracture in the foam panel was less dominant.
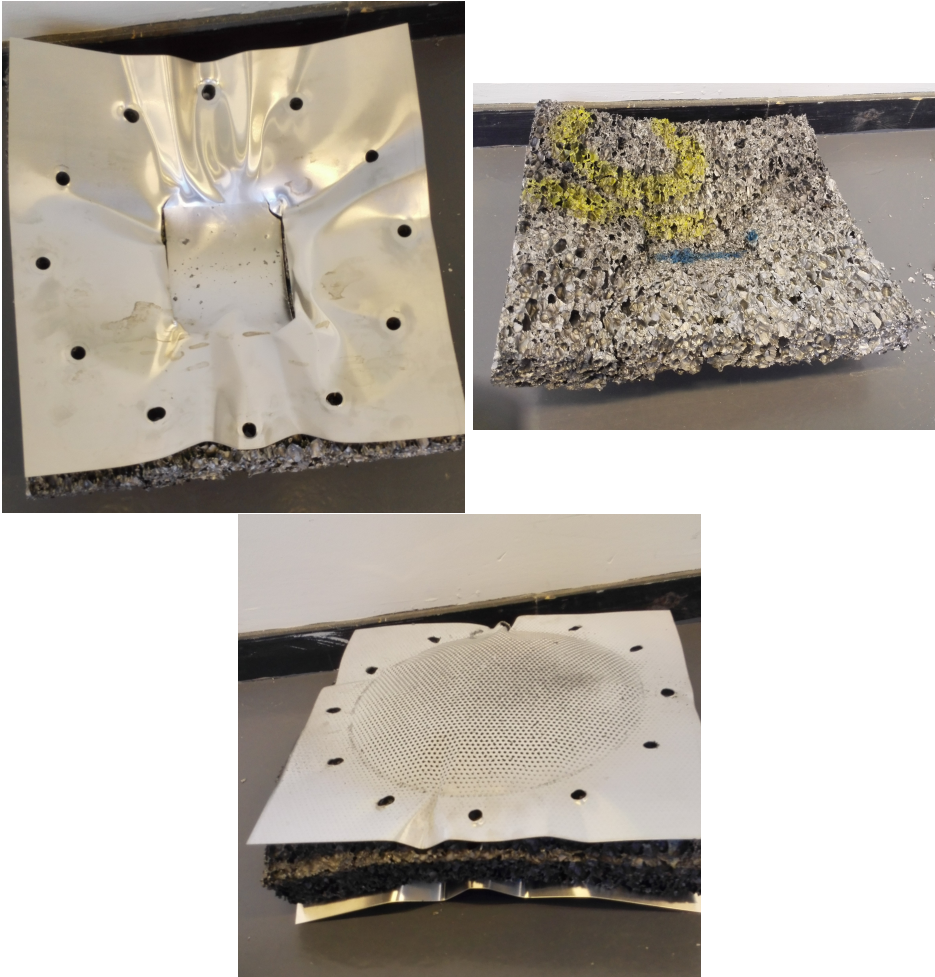
Figure 6.15: Test 1C

The top skin did not tear in test 1D. Apart from that, the deformation was similar to 1B.
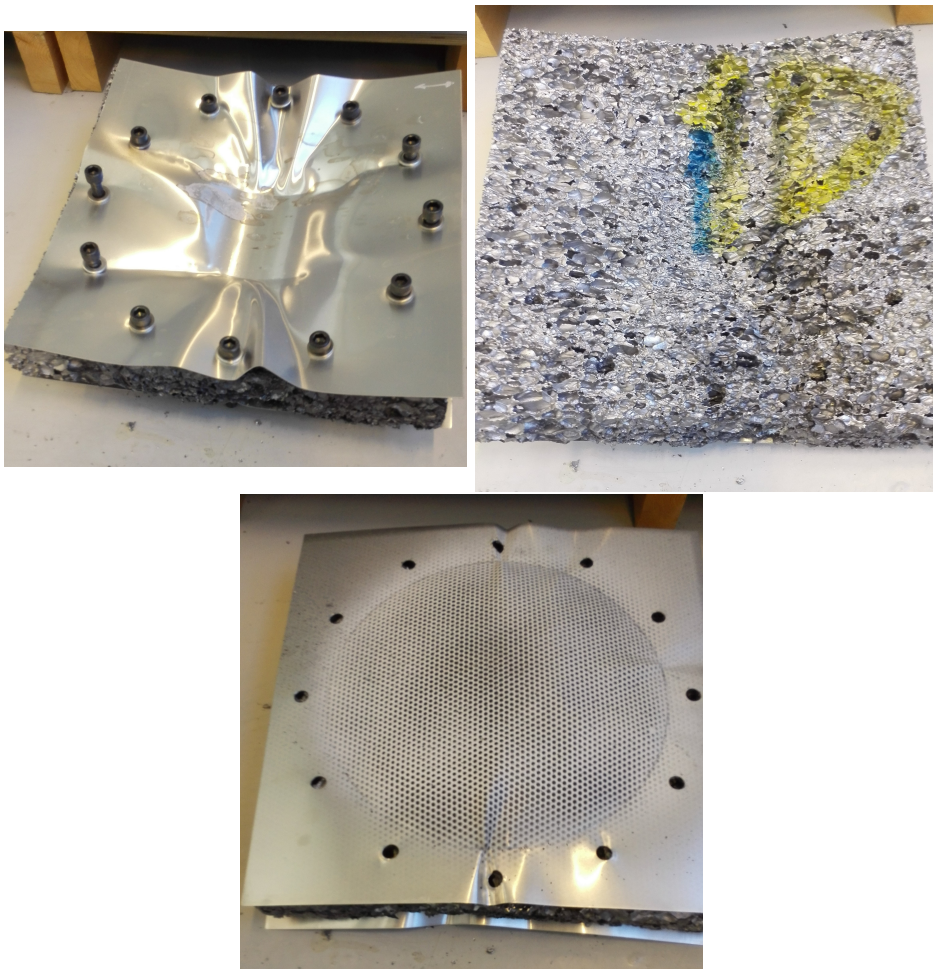
Figure 6.16: Test 1D

As seen in Figure 6.17, the failure of the foam core in 2A differed from the previous tests. The foam compressed less, but a crack through the panel was dominant. The compression of the foam was also more localised where the impactor struck. The impactor penetrated more shallow, leading to less deformation of the top skin.
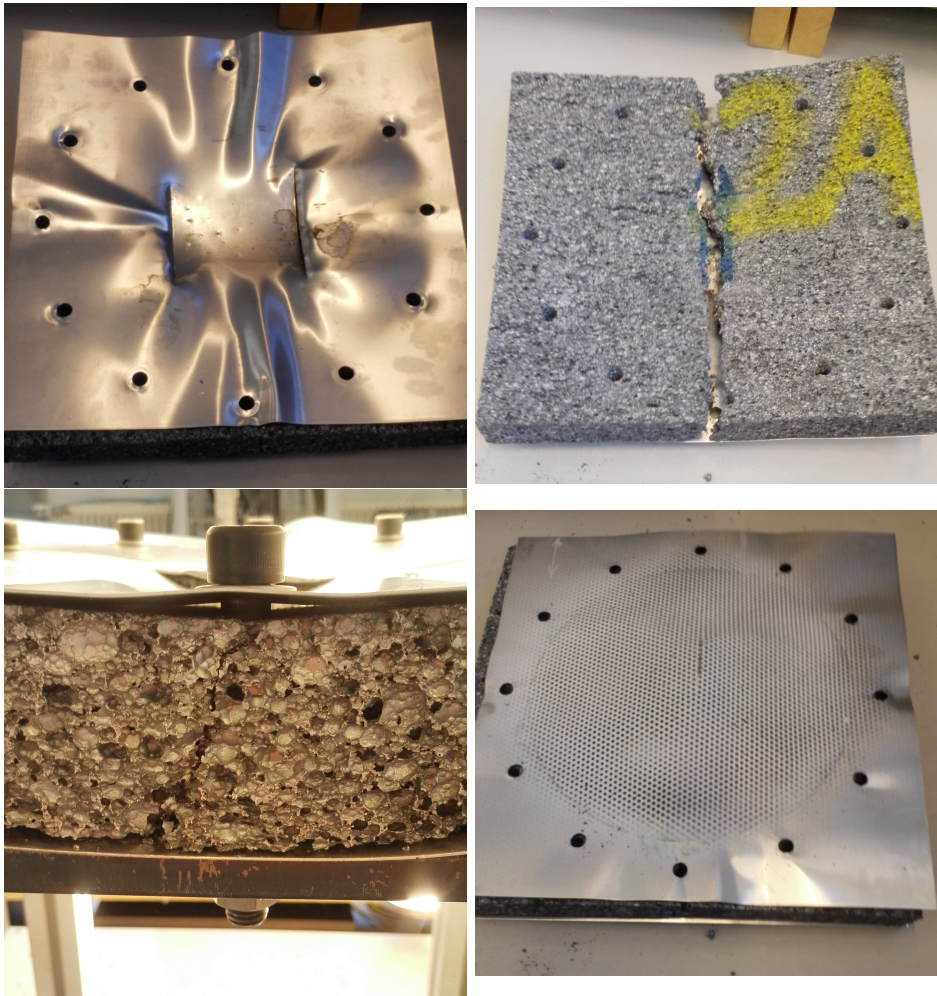
Figure 6.17: Test 2A

Also 2B differed in deformation pattern from the previous experiments. The foam core was less compressed, but there were cracks forming a cross in the rear side of the foam core. This is similar to how one could expect a solid plate to behave, though the cross is not diagonal.

Figure 6.18: Test 2B

Test 2C was the least deformed panel after impact, but once again large cracks dominate the deformation of the foam core.
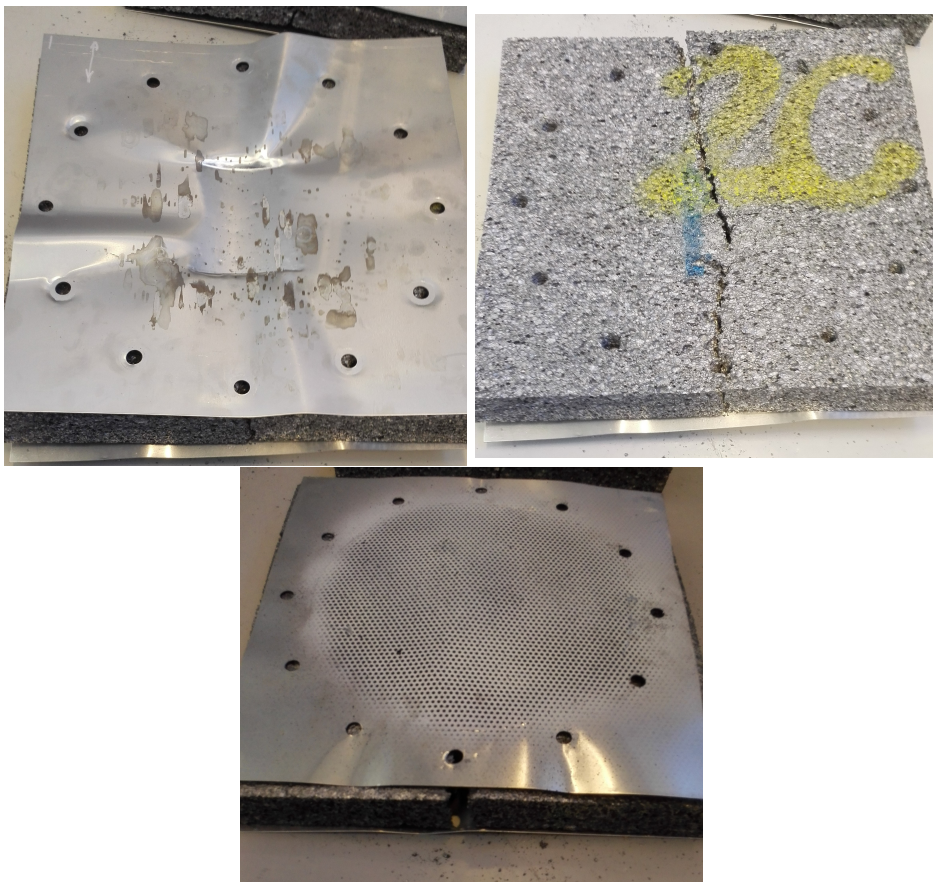
Figure 6.19: Test 2C

Test 2D was penetrated deeper than 2C, and the foam deformed locally where the impactor struck. On the rear side of the foam there was a cross-shaped crack, similar to the one in 2B. The bottom skin got a small fracture.
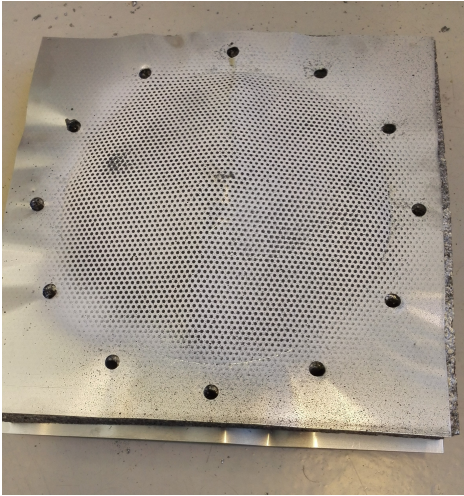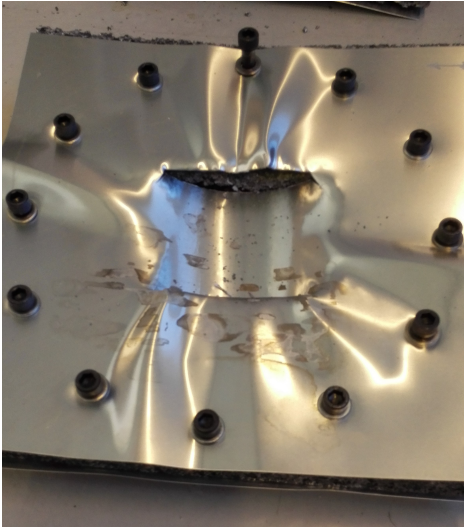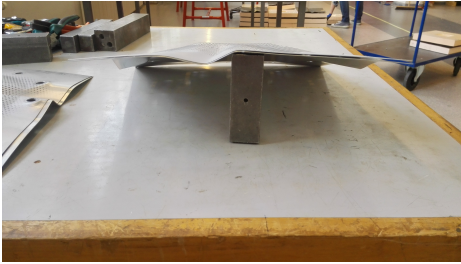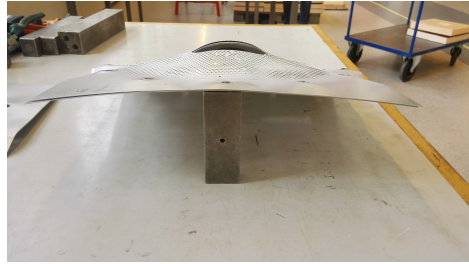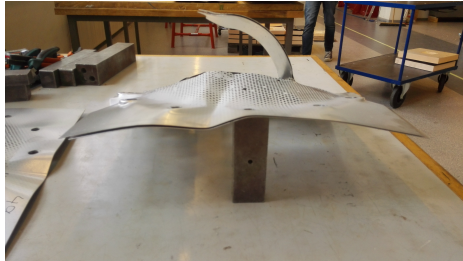
Figure 6.20: Test 2D

(a) S1

(b) S2

(c) S3

Figure 6.21: Results of Drop Tower experiments on skins without foam core
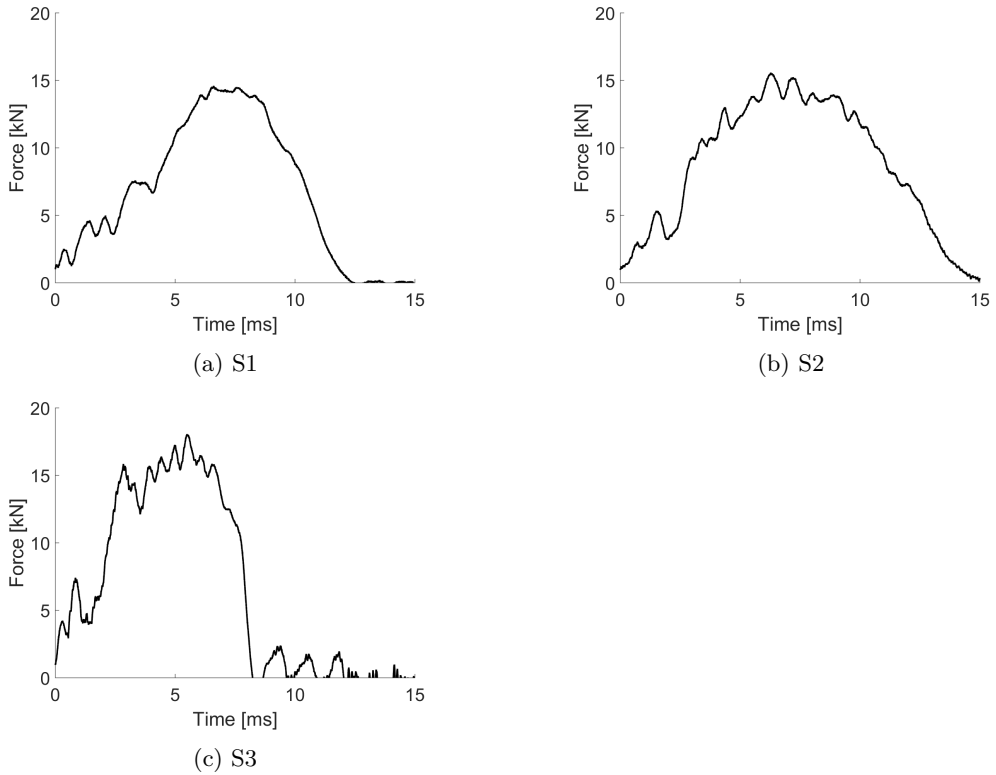
(a) S1

(b) S2

(c) S3

Figure 6.22: Force-Time for Drop Tower Experiments on Skins

For the tests on the skins only, there was no fracture in S1, while S2 and especially S3 was dominated by fracture.

In general, one can see that for the lower density, the foam seems to compress more. The denser foam seems to have the tendency to crack globally.

This impression is further enhanced when looking at the displacement of the impactor and bottom plate in Figures 6.24 and 6.25. The displacement of the bottom plate is obtained through DIC analysis, while the displacement of the impactor is calculated based on the force measurements in the striker. For the high-density foam in Series 2, the difference at peak is between 5 and 10 mm, while for Series 1 it is between 40 and 50 mm. Test 1B is not included as there was no force data obtained from this test, due to a logging error.
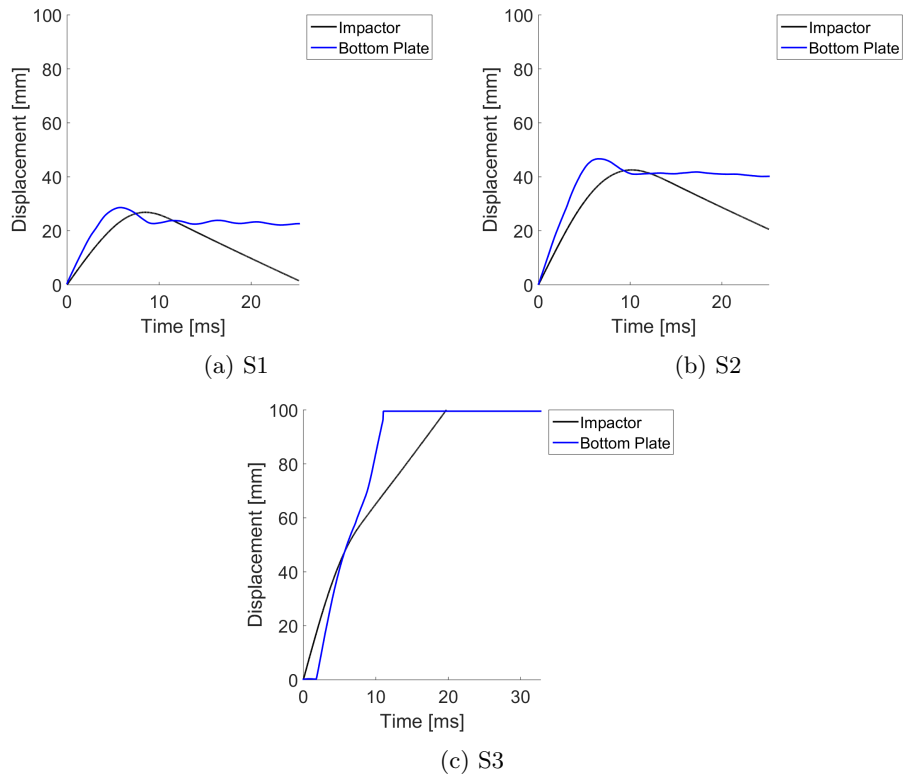
(a) S1

(b) S2

(c) S3

Figure 6.23: Displacement-Time for Drop Tower Experiments on Skins

(a) 1A

(b) 1C

(c) 1D
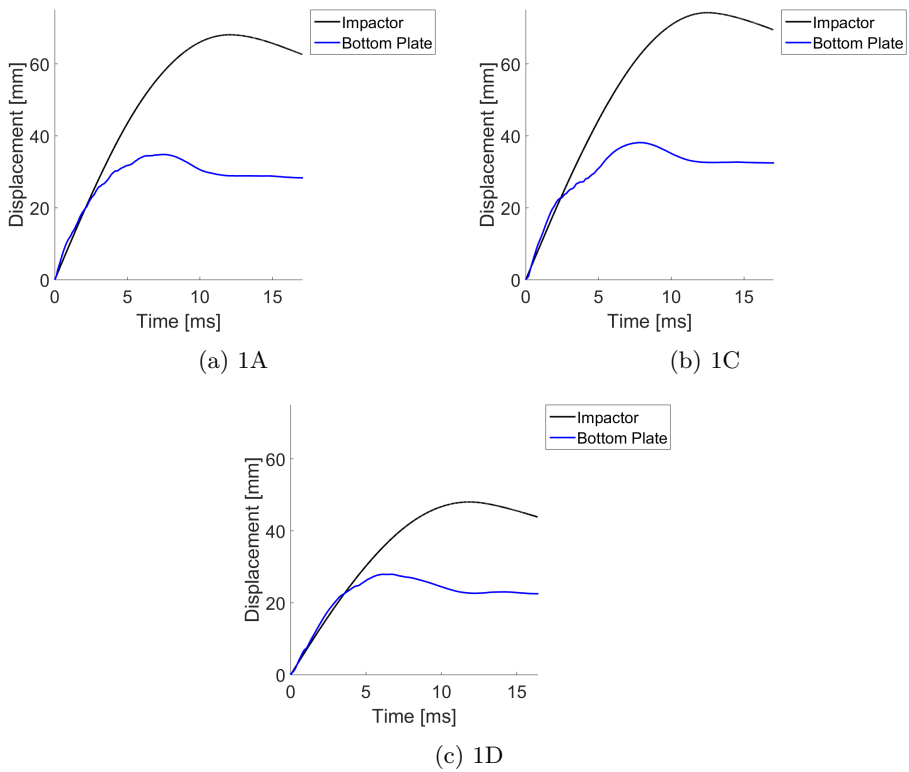
Figure 6.24: Displacement-Time for Drop Tower Experiments Series 1

Figure 6.24 shows that at first the top and bottom of the panels deform together, until a certain time where the foam cells start collapsing, and the displacement curves separate. The difference between the highest points of the two curves show the compression of the foam. In Figure 6.25 the displacement of top and bottom do not follow the same initial curve, but have different slope from the start. The final compression of the foam is smaller for these tests.

(a) 2A

(b) 2B

(c) 2C

(d) 2D

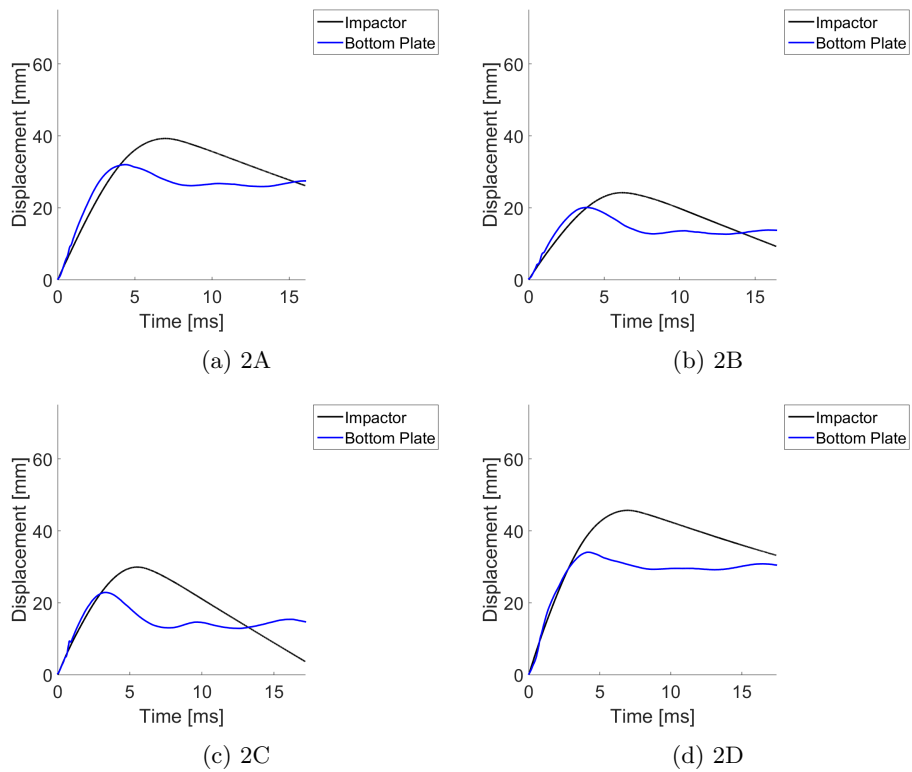Figure 6.25: Displacement-Time for Drop Tower Experiments Series 2

Figures 6.22, 6.26 and 6.27, shows significantly lower force for the lower density in Series 1 than the higher density in Series 2. There is little difference in peak force between S3 and 1A. The duration of the impact was longer for low-density foam.
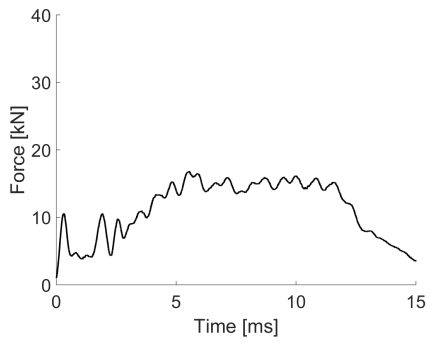
(a) 1A
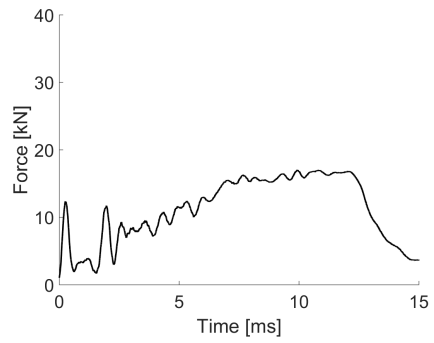
(b) 1C
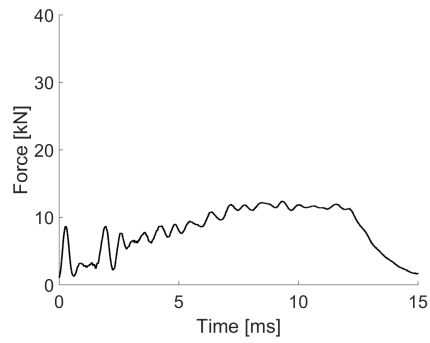
(c) 1D

Figure 6.26: Force-Time for Drop Tower Experiments Series 1

(a) 2A

(b) 2B

(c) 2C

(d) 2D
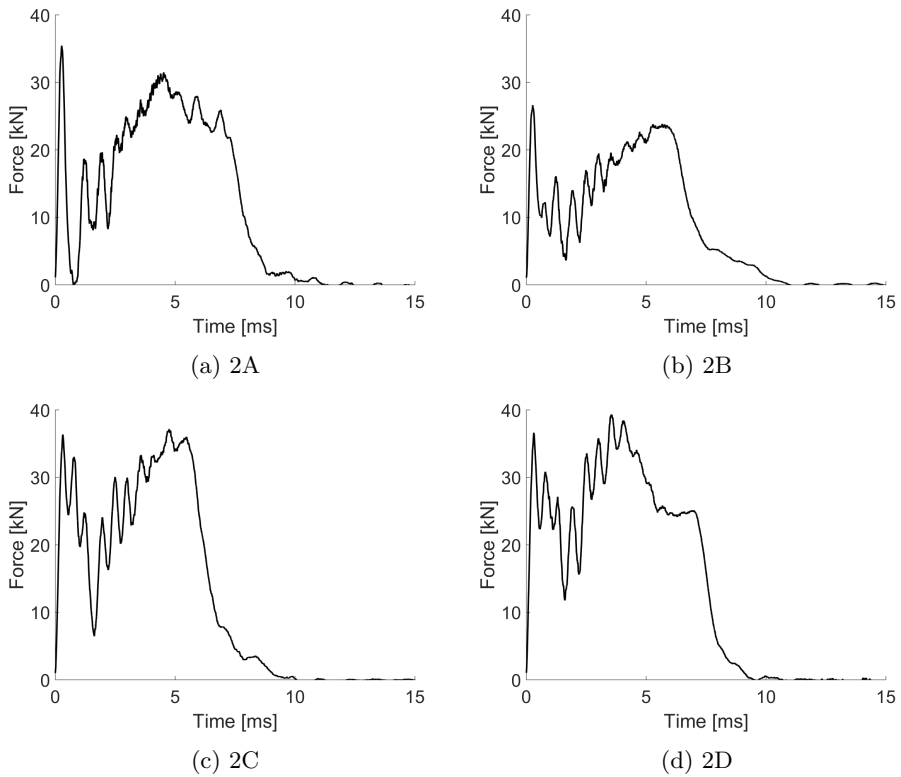
Figure 6.27: Force-Time for Drop Tower Experiments Series 2

6.2.3 Verification of analyses

To verify the analyses presented in Chapter 5 numerical analyses corresponding to the laboratory experiments have been conducted, using the model described in Chapter 4.
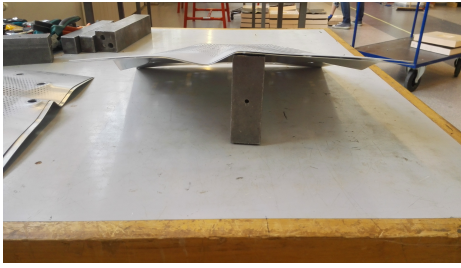
(a) S1 - Experiment
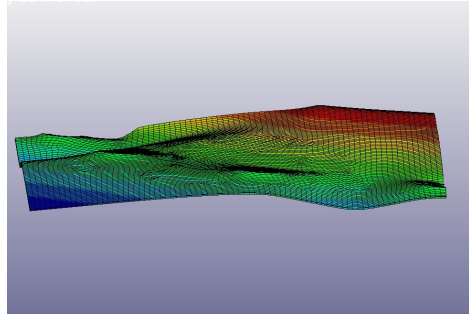
(b) S1 - Analysis
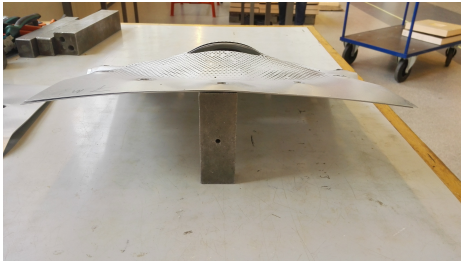
(c) S2 - Experiment
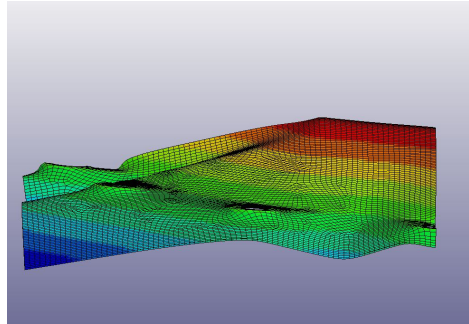
(d) S2 - Analysis
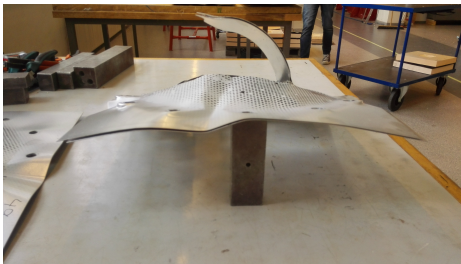
(e) S3 - Experiment
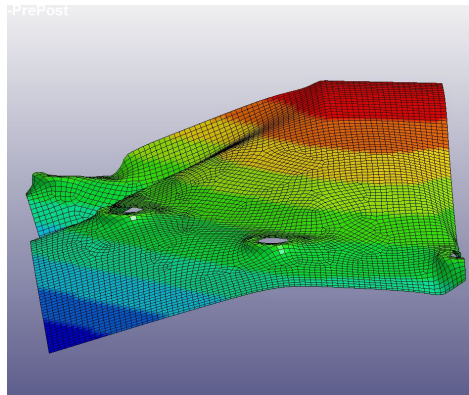
(f) S3 - Analysis

Figure 6.28: Results of Drop Tower experiments on panels without foam core compared to their numerical counterparts

From Figure 6.28, it is clear that the deformation mode of the aluminium plates are very different, as fracture has not been initated in any of the analyses. This also explains the force levels in Figure 6.29. In S1, the analysis and the experiments show similar force level, and in neither of them fracture was visible. For S2 and S3, fracture was dominant in the experiment, but not replicated in the analysis. This explains why the force level is

so far off.

(a) S1

(b) S2

(c) S3
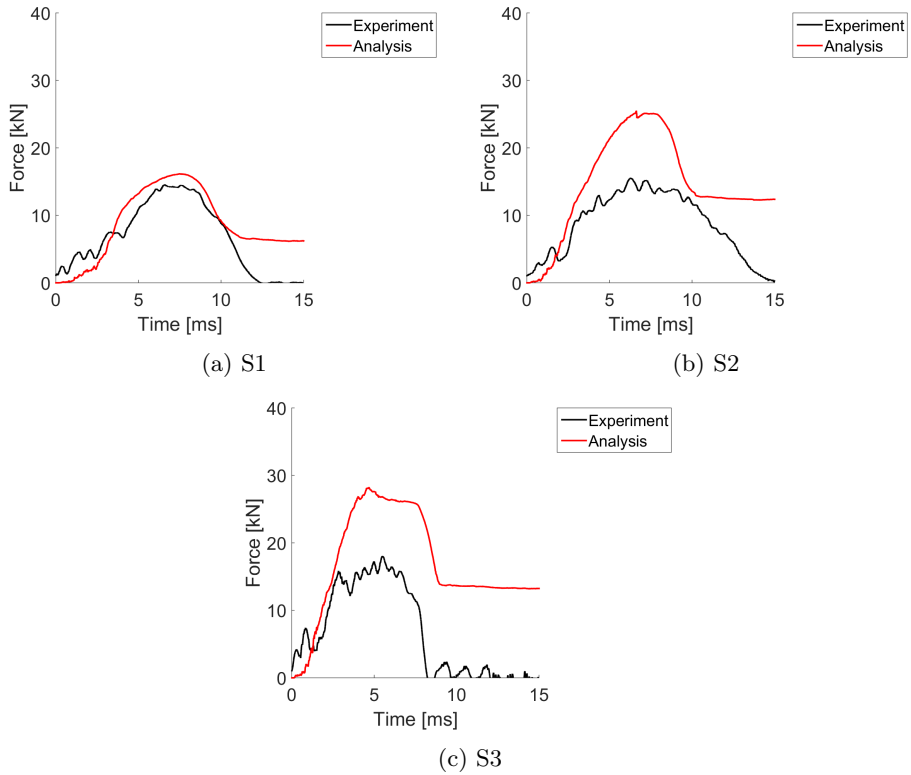
Figure 6.29: Comparision of the force levels in the experiments and analyses of the double layered panel without foam

As in Section 5.2, there was a problem with the contact formulation. Figure 6.30 shows the deviation of total energy, and shows that the internal energy is clearly higher than the kinetic energy from the impactor. The effect of this is higher for the denser foam.
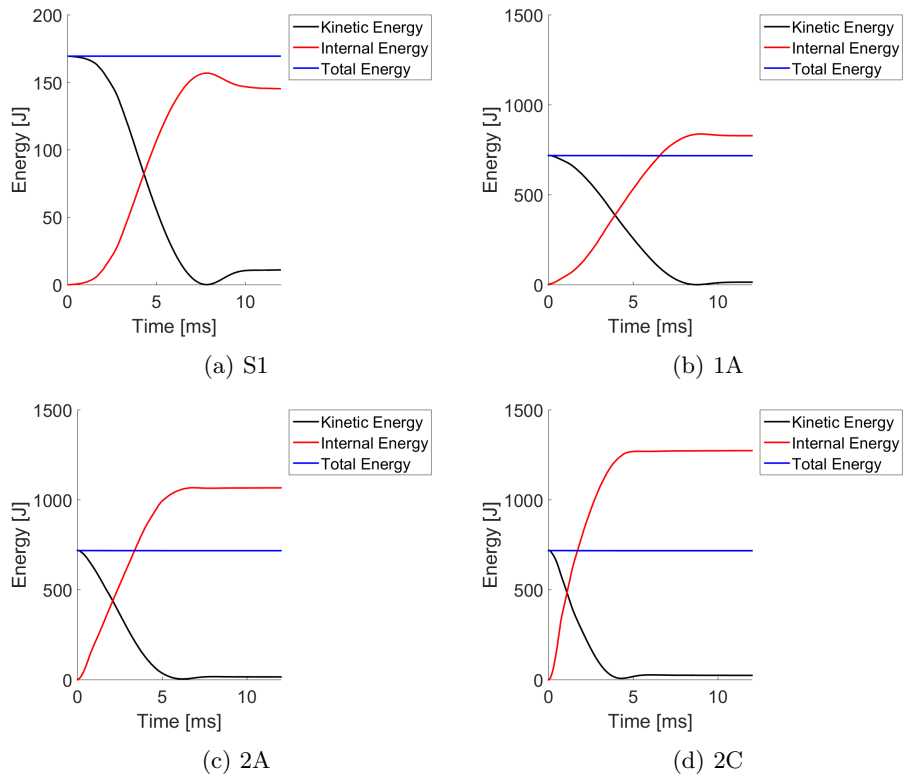
Figure 6.30: Energy levels in the analyses of the Drop Tower Experiments
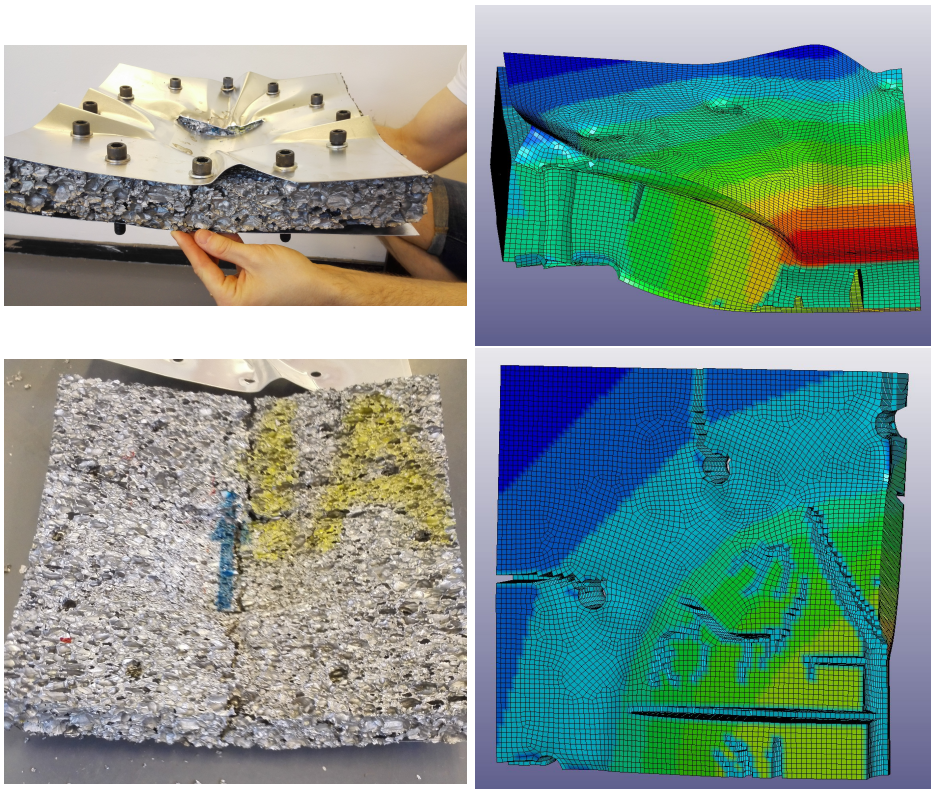
Figure 6.31: Comparision of experiment and analysis for Test 1A

Figure 6.31 shows that in both the analysis and experimental test shows significant compression of the foam core in test 1A. There are fracture lines in both experiment and analysis, though the fracture line across the centre of the specimen is further developed in the experiment. In the experiment there is fracture in the front skin, which is not replicated by the analysis.
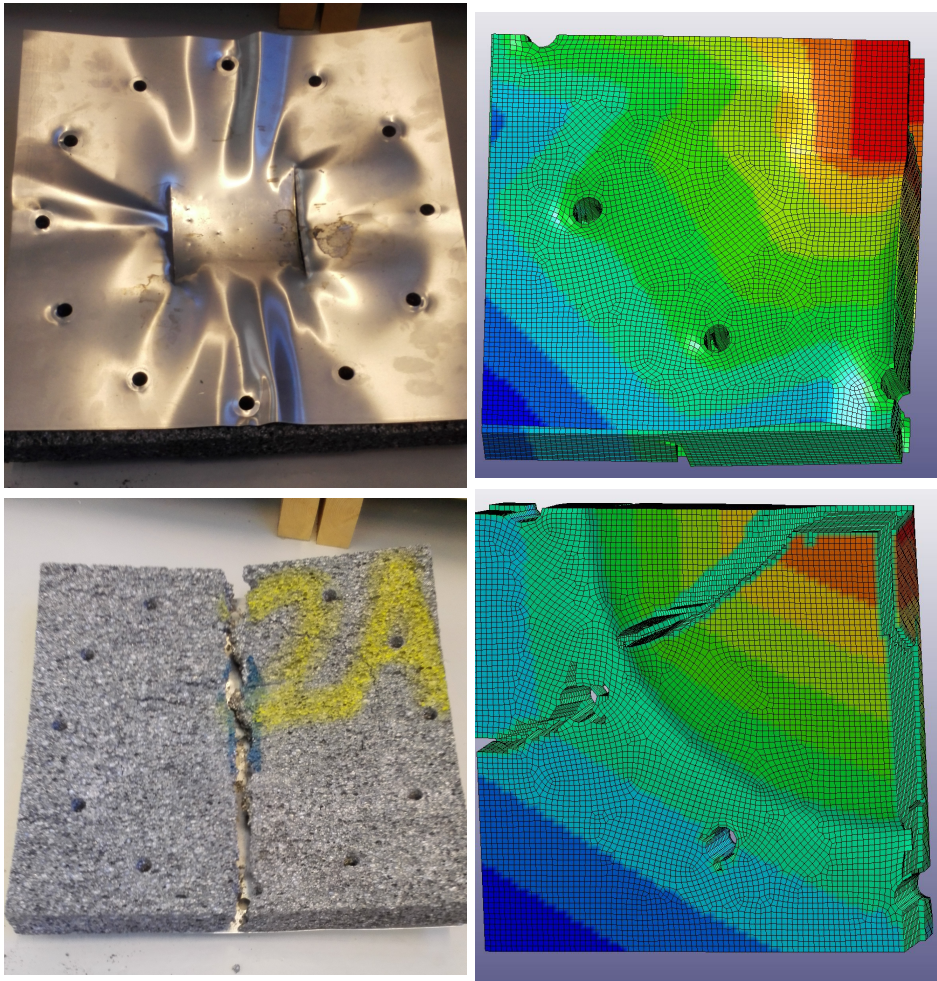
Figure 6.32: Comparision of experiment and analysis for Test 2A

As shown in Figure 6.32, there is less deformation of the foam in 2A than 1A. However, the fracture line in the foam is more distinct, which is visible in both the analysis and the experiment. In the analysis, almost all the foam is eroded along the symmetry axis, while in the experiment the foam panel broke in two. The experiment showed fracture in the front skin, which is not included in the analyses.
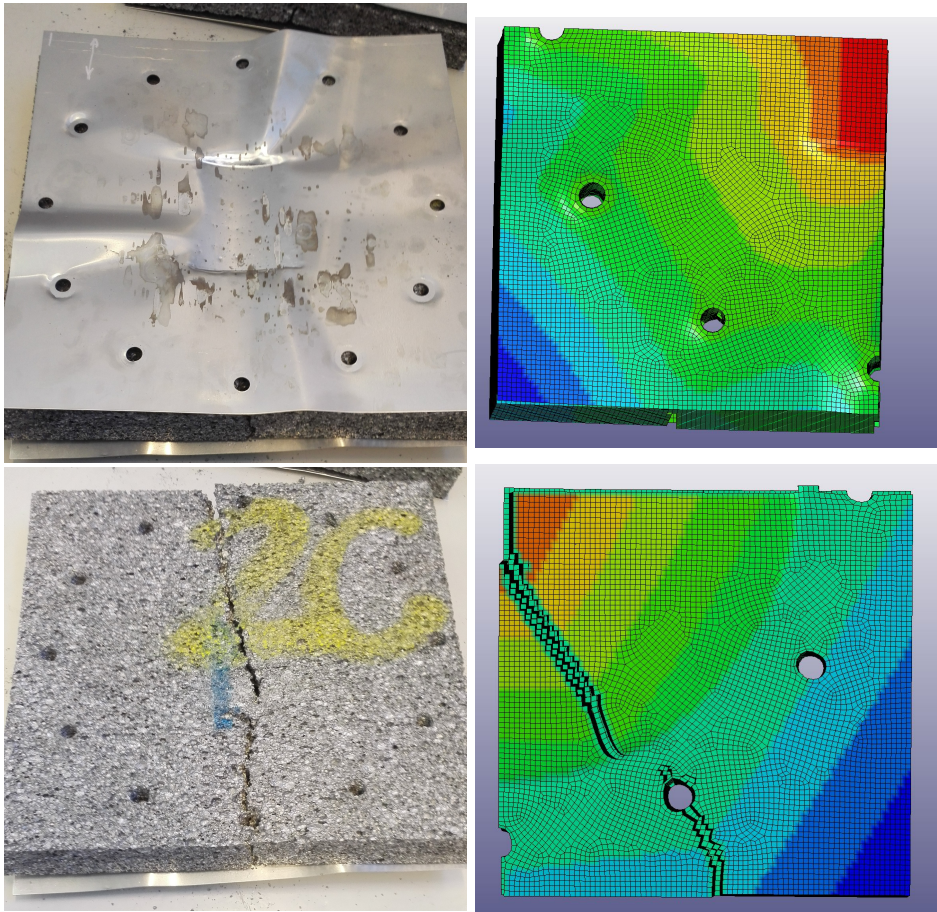
Figure 6.33: Comparision of experiment and analysis for Test 2C

In Figure 6.33, there is significantly less deformation of the foam, in both analysis and experiment. This also shows in the displacement of the bottom plate, and how far the impactor penetrated the panel. The analysis replicates a fracture line appearing in the experiment.

Table 6.6: Maximum permanent displacement of bottom skin in the Drop Tower experiment compared to their numerical counterpart

Test	Experiment [mm]	Analysis [mm]	Deviation [−]
S1	22.65	19.93	- 12.01 %
S2	40.19	29.74	- 26.00 %
1A	28.33	29.40	+ 3.78 %
2A	27.48	26.04	- 3.19 %
2C	14.70	16.18	+ 10.06 %

Table 6.6 shows the deviation between the analyses and the experiments. For the analyses with skin it is clear that the maximum displacement in the analysis is closer to the experiment for S1, where no fracture was visible in the test specimen, while it deviates significantly for S2. 1A and 2A shows small deviation, as the analysis of 1A slightly overestimates the displacement, while the opposite is true for 2A. The analysis of 2C overestimates the displacement by over 10 %.

(a) 1A

(b) S2A

(c) 2C
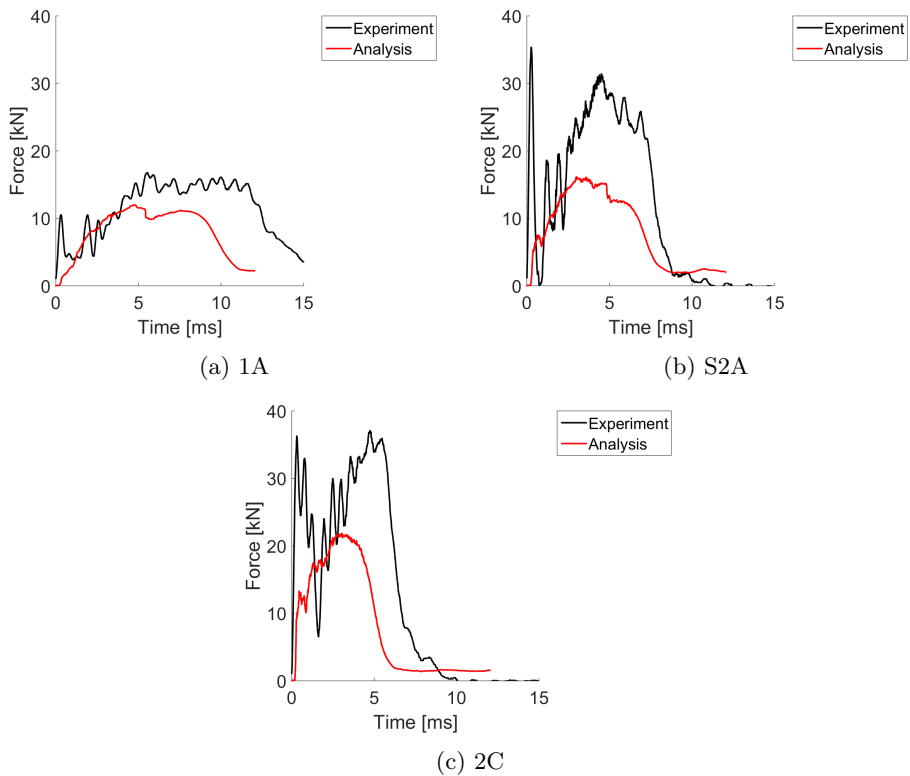
Figure 6.34: Comparision of the force levels in the experiments and analyses of the foam core sandwich panels

The force levels shown in Figure 6.34, indicates that the foam is stiffer in the experiments than in the analyses. Especially are there a high difference for 2A and 2C where the force level is twice as high in the experiments compared to the analyses.
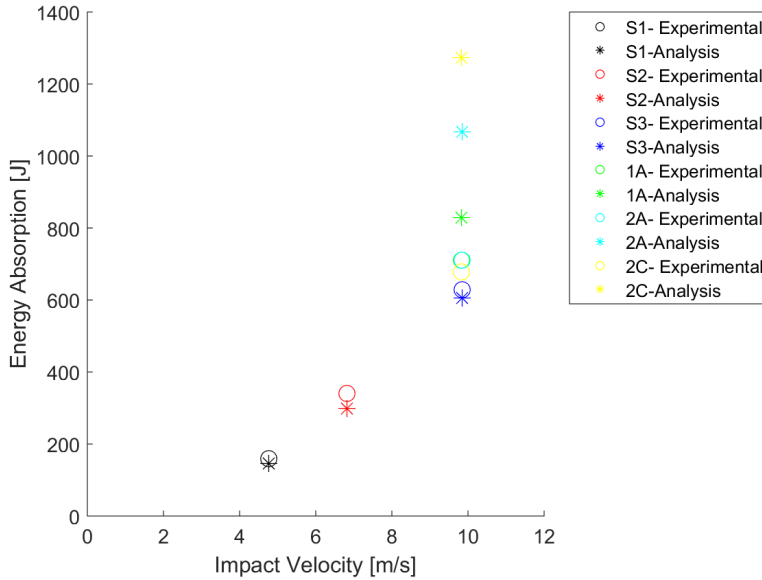
Figure 6.35: Comparision of the energy absorption in the experiments and analyses

Figure 6.35 shows that the analyses consistently underestimate the energy absorption for the foam panels, while for the panels without foam they overestimate it. It is also worth noting the the analyses show the opposite trend of the effect of foam density on the energy absorption. The analyses show more energy absorption for the denser foam, while the opposite is true for the experiments. This may be caused by the problem with the contact formulation between the foam and the skins.

Chapter 7

Results and Discussion

7.1 Blast load

The parametric studies in Section 5.1 shows that more deformation leads to higher energy absorption, as expected. The energy absorption increased as the thickness and density of the foam core decreased. The highest energy absorption per unit mass was achieved without any foam core, only the two aluminium skins. However, the experiments in Chapter 6 showed that the skins alone, would not withstand this pressure. This shows that a properly calibrated failure criterion is necessary, or else the analyses might give non-physical results.

In the parametric studies, adding a foam core lead to higher energy absorption per unit displacement.This might mean that the foam sandwich gives higher energy absorption for a given displacement.. This effect was most visible for the low-density foam, while the higher-density foam showed little improvement compared to the aluminium skins alone.

Comparing the weight-equivalent panels, indicates that to obtain the highest specific energy absorption, as light-weight panels as possible should be applied. Among the panels of the same weight those with the lowest core density absorbed most energy.

In all analyses, as well as the experiments, the maximum displacement of the rear skin was larger than the front skin. This indicates that the entire panel bends, with little compression of the foam. It might be possible to achieve higher energy absorption from the foam core by increasing the stiffness of the rear skin, or adding a support structure.

The analyses showed good correlation with the experiments, and replicated similar trends. The lack of a properly calibrated fracture criterion in the skins, might invalidate the results of the thin and light panels.

As shown in Section 5.1, it is important to adapt the thickness and foam core to the expected load. This is also pointed out by Goel et al[7]. Their study also shows that lower density leads to a faster decay of pressure, which is coherent with the results in this report.

Zhu et al. [9] finds that lower relative density of the foam leads smaller deflection of the panel, until a certain limit. This might mean that the trends shown in Section 5.1 is not complete.

Furthermore, Jang et al. [8] finds a significantly denser foam core as a result of their optimisation, underlining the importance of adapting both foam density and thickness to the expected load. They optimise for a load far higher than what has been investigated in this study.

7.2   Low-velocity impact

The experiments in Section 6.2 indicates that the lighter foam compresses more, and also that there is a larger area that is compressed. The denser plates behaves more brittle, more similar to the deformation of a plate with through-going cracks. This is reflected in the higher energy absorption calculated from the drop tower measurements on the lower-density foam.

The quantitative results of the analyses of the drop tower experiments and the parametric studies on low-velocity impact may be misleading due to the contact formulation problems. The negative energy from the contact formulation between the skins and the foam core increases in absolute value as the density of the foam core increases, and this might cause the opposite trend of what would be expected. This was realised close to finalising the study, too late to run the analyses again, as the runtime is several days. Still, the deformation modes and displacement of the tests are replicated well by the analyses, and show promise of high energy absorption for low-density foam.

Another problem with the analyses was the extrapolation of the parameters for the Deshpande-Fleck model. This means that there is no experimental evidence that the analyses replicates the correct material behaviour at the lowest density in the study of low-velocity impact. This density was only half of the lowest density studied by Hanssen [30].

As mentioned in Section 6.2, the last test (2D) revealed water inside the foam, most likely from the machining process. The constitutive model, and most theory about metal foam, is based upon the pores being filled with gas, often described by common gas laws [5]. Water is an incompressible fluid and therefore the cell volume cannot be reduced. Hence the cell-wall will stretch to compensate for their bending. The cell liquid will also add an initial stress to the cell wall, and according to Gibson and Ashby [5], this will reduce the strength of the cells by a factor of $P\left(\rho_s/\rho_f\right)$, where P is the initial pressure of the liquid.

This is further complicated by the fact that the cell faces in foams made from liquid metal often is very thin, and they might rupture, turning the closed-cell foam into a open-cell foam [5]. This leads to a very complex structure-fluid interaction problem. Guyer and Kim[36] introduced a unifying theory for the complex behaviour of porous materials, including solid-fluid interaction, solid-solid interaction and fluid-fluid interaction. Their model is, however, limited to linear-elastic solids. This makes it very difficult to estimate

the effect the pore water had on the experiments, although most contributions would likely lead to a stiffer behaviour.

Chapter 8

Conclusions and Further Work

Foam core sandwich panels show potential for increasing the energy absorption, especially when one of the objectives of the structure is to limit the deformation.

However, the parametric studies needs to be conducted with a correct failure criterion in the aluminium skins in order to be sure that the structure will withstand the applied blast load, and to validate the results.

The highest energy absorption per unit mass was achieved by the skins alone, though they would break at the given blast load. Therefore, the response of monolithic aluminium plates of equivalent mass should be compared to the sandwich panels. It could also be interesting to compare the panels to the minimum-weight monolithic plates that would withstand the load.

Another option would be to increase the stiffness of the rear skin, to obtain more compression of the foam core. However, the extra mass added needs to be taken into account.

The parametric study should be conducted with limitations taken from given applications. For example, the panels should be optimised towards a maximum displacement or the ability to withstand a certain blast load.

For the case of low-velocity impact, the experimental tests showed potential for increasing the energy absorption by introducing a foam core. However, new experiments should be conducted to obtain data of the response of the higher density foam without pore liquid.

The parametric studies should also be conducted with proper contact formulations to obtain numerical data on the response of the sandwich panels. In order to obtain reliable data for these parametric studies, the Deshpande-Fleck model should be calibrated and validated for the densities used in the parametric studies, to ensure that the range of the interpolation is valid.

References

[1] Norwegian Police Security Service, *Annual Threat Assessment 2015*, 2015. [http://www.pst.no/media/utgivelser/annual-threat-assessment-2015/ ; accessed 04-April-2016].

[2] The Norwegian Defence Estates Agency, *For et tryggere Norge*, 2016. [http://www.forsvarsbygg.no/globalassets/documents/nksb/nksb-180x180-visning.pdf ; accessed 04-April-2016].

[3] T. Børvik, O. S. Hopperstad, and M. Langseth, "Lecture Notes in TKT4128 - Impact Mechanics: An Introduction to Penetration and Perforation Mechanics." NTNU 2015.

[4] V. Aune, T. Børvik, and M. Langseth, "Lecture Notes in TKT4128 - Impact Mechanics: An Introduction to Blast Mechanics." NTNU 2015.

[5] L. J. Gibson and M. F. Ashby, *Cellular Solids - Structure and Properties*. Cambridge University Press, 1999.

[6] F. Zhu, L. Zhao, G. Lu, and Z. Wang, "Structural response and energy absorption of sandwich panels with an aluminium foam core under blast loading," *Advances in Structural Engineering*, vol. 11, pp. 525–536, 2008.

[7] M. Goel, P. Altenhofer, V. Matsagar, A. Gupta, C. Mundt, and S. Marburg, "Interaction of a shock wave with a closed cell aluminum metal foam," *Combustion, Explosion and Shock Waves*, vol. 51, no. 3, pp. 373–380, 2015. cited By 0.

[8] S. Jang, Y. Park, and H.-J. Choi, "Integrated design of aluminum foam processing parameters and sandwich panels under uncertainty," *Proceedings of the Institution of Mechanical Engineers, Part C: Journal of Mechanical Engineering Science*, vol. 229, no. 13, pp. 2387–2401, 2015.

[9] F. Zhu, Z. Wang, G. Lu, and L. Zhao, "Analytical investigation and optimal design of sandwich panels subjected to shock loading," *Materials and Design*, vol. 30, no. 1, pp. 91–100, 2009.

[10] "LS-DYNA Keyword User's Manual Volume II," 2015.

[11] W. D. Callister and D. G. Rethwisch, *Material Science and Engineering - An Introduction*. John Wiley & Sons Inc., 7 ed., 2007.

[12] Standard Norge, *NS-EN573-1:2004: Aluminium and aluminium alloys - Chemical composition and form of wrought products - Part 1: Numerical designation system*, 2005.

[13] Standard Norge, *NS-EN573-3:2013: Aluminium and aluminium alloys - Chemical composition and form of wrought products - Part 3: Chemical composition and form of products*, 2013.

[14] Standard Norge, *NS-EN515:1993: Aluminium and aluminium alloys - Wrought products - Temper designations*, 1993.

[15] Wikipedia, "Metal foam — Wikipedia, the free encyclopedia," 2016. [Online; accessed 03-June-2016].

[16] T. Børvik, O. S. Hopperstad, A. Reyes, M. Langseth, G. Solomos, and T. Dyngeland, "Empty and foam-filled circular aluminium tubes subjected to axial and oblique quasistatic loading," *International Journal of Crashworthiness*, vol. 8, no. 5, pp. 481–494, 2003.

[17] A. Hanssen, M. Langseth, and O. Hopperstad, "Optimum design for energy absorption of square aluminium columns with aluminium foam filler," *International Journal of Mechanical Sciences*, vol. 43, no. 1, pp. 153 – 176, 2001.

[18] A. G. Hanssen, K. Stöbener, G. Rausch, M. Langseth, and H. Keller, "Optimisation of energy absorption of an a-pillar by metal foam insert," *International Journal of Crashworthiness*, vol. 11, no. 3, pp. 231–242, 2006.

[19] A. Hanssen, Y. Girard, L. Olovsson, T. Berstad, and M. Langseth, "A numerical model for bird strike of aluminium foam-based sandwich panels," *International Journal of Impact Engineering*, vol. 32, p. 1127–1144, 2006.

[20] A. Hanssen, L. Enstock, and M. Langseth, "Close-range blast loading of aluminium foam panels," *International Journal of Impact Engineering*, vol. 27, no. 6, pp. 593–618, 2002.

[21] SecretDisc. https://commons.wikimedia.org/w/index.php?curid=3360395.

[22] Stehfun. https://commons.wikimedia.org/w/index.php?curid=2971205.

[23] C. Foo, L. Seah, and G. Chai, "Low-velocity impact failure of aluminium honeycomb sandwich panels," *Composite Structures*, vol. 85, no. 1, pp. 20–28, 2008.

[24] T. Zhang, Y. Yan, and J. Li, "Experiments and numerical simulations of low-velocity impact of sandwich composite panels," *Polymer Composites*, 2015.

[25] V. Aune, M. Langseth, and T. Børvik, "Behaviour of plated structures subjected to blast loading," *EPJ Web of Conferences*, vol. 94, 2015.

[26] J. K. Holmen, O. S. Hopperstad, and T. Børvik, "Low-velocity impact on multi-layered dual-phase steel plates," *International Journal of Impact Engineering*, vol. 78, pp. 161–177, 2015.

[27] E. Fagerholt, T. Børvik, and O. Hopperstad, "Measuring discontinuous displacement fields in cracked specimens using digital image correlation with mesh adaptation

and crack-path optimization," *Optics and Lasers in Engineering*, vol. 51, no. 3, pp. 299–310, 2013. cited By 18.

[28] T. Børvik, O. Hopperstad, T. Berstad, and M. Langseth, "A computational model of viscoplasticity and ductile damage for impact and penetration," *European Journal of Mechanics - A/Solids*, vol. 20, pp. 685–712, 2001.

[29] C. Baglo and T. M. Dybvik, "Experimental and numerical study on plated structures subjected to blast loading," Master's thesis, NTNU, 2015.

[30] A. Hanssen, O. Hopperstad, M. Langseth, and H. Ilstad, "Validation of constitutive models applicable to aluminium foams," *International Journal of Mechanical Sciences*, vol. 44, no. 2, pp. 359–406, 2002. cited By 209.

[31] A. Reyes, O. Hopperstad, T. Berstad, A. Hanssen, and M. Langseth, "Constitutive modeling of aluminum foam including fracture and statistical variation of density," *European Journal of Mechanics, A/Solids*, vol. 22, no. 6, pp. 815–835, 2003. cited By 84.

[32] V. Deshpande and N. Fleck, "Isotropic constitutive models for metallic foams," *Journal of the Mechanics and Physics of Solids*, vol. 48, no. 6, pp. 1253–1283, 2000. cited By 547.

[33] V. Deshpande and N. Fleck, "High strain rate compressive behaviour of aluminum alloy foams," *International Journal of Impact Engineering*, vol. 24, no. 3, pp. 277–298, 2000. cited By 344.

[34] D. K. Rajak, L. Kumaraswamidhas, S. Das, and S. S. Kumaran, "Characterization and analysis of compression load behaviour of aluminium alloy foam under the diverse strain rate," *Journal of Alloys and Compounds*, vol. 656, pp. 218 – 225, 2016.

[35] A. Tømte, "Energy absorption and damage prevention in a submerged floating tunnel during internal blast loading," Master's thesis, NTNU, 2015.

[36] R. Guyer and H. Kim, "Theoretical model for fluid-solid coupling in porous materials," *Physical Review E - Statistical, Nonlinear, and Soft Matter Physics*, vol. 91, no. 4, 2015.

Appendix A

Appendix

A.1   Aluminium Plates - Material Card

**Hydro Aluminium
Rolled Products**

NO 104701
ASTRUP A.S
HAAVARD MARTINSENS VEI 34
0978   OSLO
Norway

Inspection Certificate no: KRM 105428 - 1

According to EN 10204 - 3.1.

Date   : 11/05/2015   Page : 1

Customer order no	: 1258898
Our order no	: 583972-1
Invoice no	:
Packing list no	: KRM105428
Product	: 0.800 x 1250 x 2500
Gross weight	: 6263 Kg
Net weight	: 6059 Kg
Customer part no	:
Alloy/temper	: 105025 14
Customer Spec.	:

	Si	Fe	Cu	Mn	Mg	Zn	Ti	Al
Min								99.50
Max	0.25	0.40	0.05	0.05	0.05	0.07	0.05	
434565	0.04	0.32	0.001	0.002	0.000	0.000	0.020	99.62

Mechanical properties

	Rp0.2	Rm	Elong A50			Thick-ness				
Cust. Min	85	105	2			0.740				
Max		145				0.860				
Coil no. 434565	110	120	5			0.790				

Material Specification and Test Results
Standard EN 485/515/573

Test Direction   : Transverse

Kristian Stray   (sign.)
Plant Metallurgist

Astrup AS 13/05/15 sgi
1258898/1   105